International Journal of Heat and Mass Transfer 267 (2026) 128972

Contents lists available at ScienceDirect

International Journal of Heat and Mass Transfer

journal homepage: www.elsevier.com/locate/ijhmt

The influence of thermal radiation absorption on the interaction of transient transfer processes for a water droplet evaporating in a high-temperature gas flow

Gintautas Miliauskas [a], Monika Maziukiene [a], Robertas Poškas [a,b], Egidijus Puida [a], Hussam Jouhara [c,*]

[a] Department of Energy, Kaunas University of Technology, Studentu 56, LT-51424 Kaunas, Lithuania
[b] Nuclear Engineering Laboratory, Lithuanian Energy Institute, Breslaujos 3, LT-44403 Kaunas, Lithuania
[c] Heat Pipe and Thermal Management Research Group, College of Engineering, Design and Physical Sciences, Brunel University London, Uxbridge UB8 3PH, United Kingdom

ARTICLE INFO

Keywords:
High temperature gas flow
Water droplet
Phase change
Transient transfer processes
Thermal radiation

ABSTRACT

This work presents a study of transient transfer processes of water droplets evaporating in flue gas, including spectral radiation absorption and droplet slip. The results of numerical modelling of condensation, transitional and equilibrium evaporation regimes of water droplets in flue gas at temperatures ranging from 633 to 1833 K are presented. The modelled radiative transfer is based on geometrical optics theory. Convective heating and evaporation of the droplet are defined by the empirical Clift correlation for Reynolds numbers Re $<$ 400. The interaction between transient processes and the dependence of the physical and optical spectral properties of a warming droplet on temperature are taken into account. The numerical iterative scheme defining the average instantaneous temperature of the droplet's surface and working according to the fastest descent method is based on the balance of heat fluxes. The influence of Stefan flow, evaluated by the Spalding heat- and mass-transfer parameters, is made universal for different droplet phase change regimes by carefully assessing the dynamics of the temperature gradient within the droplet. It was verified that the competing effects of droplet slipping and the absorption of radiation are essential for the interaction between droplet transfer processes. The internal heat transfer in a droplet is affected by absorbed radiation and influenced by water circulation. Due to the effect of absorbed radiation, the evaporation rate of a large water droplet more than doubles in flue gas at 818 K and increases up to fourfold at 1133 K. These simulation results agree with the experimental data.

1. Introduction

The heat and mass transfer of water droplets is relevant to atmospheric phenomena and industrial water spraying for various technological purposes. Dispersed water is used for fire suppression [1], for reducing the concentration of toxins in boilers [2–4], for flue gas temperature regulation [5] and heat recovery [6]. Spraying water into the furnace leads to longer flames and a stabilised combustion process and a lowered combustion temperature effectively inhibits the formation of thermal nitrogen oxides [2]. The spray of sorbents and ammonia with water droplets into flue gas of a certain temperature also ensures a significant reduction of already formed nitrogen oxides [3].

In cogeneration power plants the water spray not only into furnace and into exhaust flue gas flow, but also into combustion air flow [7] and into condensing economiser [6]. In the first three cases, droplet evaporation is important, whereas in the contact-type condensing economiser heat is recovered from the flue gas through the process of vapour condensation on the droplets. In order to develop efficient water spraying technologies, it is essential to know the details of the droplet phase change processes and to take them into account in practice under various boundary conditions. Studies on the heat and mass transfer of single liquid droplets are important for explaining general patterns of phase change in dispersed liquids and the interaction of complex's heat and mass transfer processes can also play a role in the thermal technologies. Therefore, the heat and mass transfer of liquid droplets and their spraying systems have been studied for over a century, and the

* Corresponding author.
E-mail address: Hussam.Jouhara@brunel.ac.uk (H. Jouhara).

https://doi.org/10.1016/j.ijheatmasstransfer.2026.128972
Received 17 October 2025; Received in revised form 16 April 2026; Accepted 8 May 2026
Available online 14 May 2026

results of such studies are comprehensively reviewed and summarised in monographs [8–16] inter alia.

Initially, the evaporation of water and pure fuel droplets was studied in atmospheric air [8]. The boundary conditions were then extended to include other fluids and their mixtures, and the ambient gas temperature was significantly increased [9], taking into account the influence of radiation [10,11]. Empirical computational methods for estimating the influence of the Stefan flow on convective heating and evaporation of a droplet have been developed [12], based on the Spalding heat and mass transfer parameters [17]. Attention has been drawn to the importance of disperse systems in engineering applications and to the peculiarities of complex transfer processes occurring in them [12–14]. The importance of phase changes transitional regimes and the effect of spectral radiation absorption on the evaporation of semi-transparent droplets is justified [13,14]. Heat transfer via external thermal radiation in a heated droplet cloud is affected by radiation attenuation within the droplet layer. Both absorption and anisotropic scattering of radiation by droplets are responsible for this effect [13]. Radiation propagation in an absorbing and scattering medium is described by the integro-differential radiative transfer equation (RTE), in which the integral term is responsible for the anisotropic scattering of radiation [18]. Significant mathematical difficulties associated with scattering anisotropy are overcome in the case of multiple scattering by the use of the so-called transport approximation recommended in [13,19]. The analytical methods for modelling droplet evaporation are also being improved, providing mathematical tools needed to generalise transport and constitutive equations and to find analytical solutions in curvilinear coordinate systems [15]. A rigorous approach to the evaporation problem in a two-phase flow based on the solution of heat and mass transfer equations inside and outside an individual droplet in a system that includes millions of droplets (e.g. sprays in internal combustion engines, water droplet mist curtains for shielding from flame radiation) is practically out of the question for realistic engineering spray applications [16]. This has stimulated the development of many simplified models of the relevant processes for CFD codes [16].

Radiation absorption in fuel and water droplets is most often described by spectral models based on Mie theory [10,11,19–27, et. al.], which allows for the analysis of volumetric radiation absorption independently of the droplet's dispersity. The intense ambient thermal radiation has a significant effect on the interaction between the combined heat transfer processes in semi-transparent liquid droplets and their thermal state [21,28,29] and increases the evaporation rate [2,20,30]. For droplets of liquid mixtures and solutions, it can cause a non-monotonic variation in their temperature [26] or even induce an explosive evaporation regime [31].

The significant influence of the absorbed radiation on the equilibrium evaporation rate of water droplets was confirmed in [20] by modelling the evaporation of a falling 373 K water droplet in a high-temperature gas, when a spectral black source with temperature $T_{sour} = T_g$ radiated. The effect of Stefan flow on the external convective heating of an evaporating droplet is evaluated by the universal model of the Spalding heat transfer parameter B_T:

$$B_T = c_{p,v,vg}\frac{T_g - T_R}{L - q/m_v}, \text{when} q = q_f - q_{c,g} \tag{1}$$

The effect of the temperature gradient is neglected and, in the case of equilibrium evaporation, the heat flux q in expression (1) is equated to the thermal radiation flux q_r absorbed by the droplet, which is defined by the effective absorptance coefficient of the droplet α_{ef} [20]:

$$q_r = \alpha_{ef}(T_g)\sigma T_g^4 - \alpha_{ef}(T_s)\sigma T_s^4 \tag{2}$$

because the droplet emissivity is $\alpha_{ef}(T_s)$ according to Kirchhoff's law. The water droplet effective absorption $\alpha_{ef} \equiv 0 \rightarrow 0.934$ has been calculated by the spectral model of Mie theory and tabulated, when the droplet diameter $2R \equiv 0 \rightarrow \infty$, for radiating source temperatures in the interval $T_{sour} \equiv 373 \rightarrow 1450$ K. The beam tracing procedure for Mie theory developed for these computations includes polarisation, refraction, external reflection, multiple internal reflection, and absorption by the spectral complex refractive index of the water [32,33].

For various liquid spray technologies, the droplet's transient evaporation regime is of great importance. In these cases, not all of the heat supplied to the droplet participates in the liquid evaporation process and this must be taken into account in Eq. (1) [34]. Then, when calculating the Spalding parameter according to the Eq. (1), the influence of the temperature gradient change in the droplet must be taken into account [29]. The indicates a close connection between the external and internal transfer processes in a droplet. In the case of radiative-conductive heat transfer, the temperature gradient in a spherical semi-transparent droplet is described by an integral model in work [35]. The iterative solution method of droplet evaporation, which is based on the balance of heat fluxes of a droplet and the determination of the average instantaneous temperature of its surface by iterative calculations, is also presented [35]. Importantly, in the case of iterative calculations the problems of droplet evaporation, external heating and internal heat transfer can be considered relatively independent. This allows the model for each problem to be improved independently of the others. Based on the effective thermal conductivity parameter model [36],

$$k_{ef} = 1.86 + \tanh\left(2.245\log_{10}\frac{\mathrm{Pe}_l}{30}\right) \tag{3}$$

a model of the inner radiative-conductive heat transfers [35] has been refined in [37] to take into account the influence of the liquid forced circulation and to carefully consider the dependence of the physical properties of the liquid temperature. However, this model allows us to evaluate the interaction of complex heat transfer processes in a droplet only when the local radiative flux in it is known. The local absorption of infra-red radiation in large- and medium-sized semitransparent droplets can be described by spectral models based on the theory of geometric optics [2,35]. In [24] it is suggested that droplets with the diameter of $2R > 100$ μm should be considered as medium-sized or large-sized droplets. Such a classification requires verification. This can be done by comparing the results of modelling the absorbed radiation flux of water droplets by spectral model based on the theory of geometric optics with the data obtained by Harpole according to Eq. (2). Numerical models for the evaporation of liquid droplets and sprays are constructed using simplifying assumptions. Therefore, the validation of these models requires a comparative assessment of the correspondence of numerical results to experimental data. Modern measurement capabilities allow the investigations of heat and mass transfer processes of liquid droplets under a wide range of boundary conditions [38–45, et. al.]. In thermal spray technologies, the evaporation rate of droplets is very important. In this respect, the experimental study [45] can be considered as unique since the evaporation rate of a water droplet in a high-temperature radiant environment was measured directly. The water droplet with the equivalent diameter of $2R \equiv 0.4 \rightarrow 3.2$ mm was suspended on a thermocouple bead in high-temperature air at 405→860 ℃, and heated water was supplied to it through a glass capillary. The iron wall enclosing the air was radiating, and the vapour-air mixture was being ejected at a velocity of 0.01 m/s. Therefore, combined heating of the droplet was taking place by radiation and convection and the conditions $T_{sour} = T_g$ and $\mathrm{Re} < 0.3$ were valid. The equilibrium evaporation rate of the droplet ($g_{v,e} \equiv (0.5 \rightarrow 11)\ 10^{-7}$ kg/s) was equated to the capillary-fed water flow rate when the droplet temperature stopped changing and the droplet projection on the screen stabilised. These experimental data are defined with 95% confidence [45] and are important for validating the reliability of theoretical droplet evaporation models. Part of these data is presented in [28] and evaluated in works [2,37,46].

In summary, the absorption of spectral radiation in semi-transparent droplets, their slipping and the effect of Stefan flow are essential factors in determining the evaporation rate of sprayed liquid droplets. The

influence of these factors on the equilibrium evaporation of fuel and water droplets is well known, but their effect on the transient phase change regimes has not been studied in sufficient detail. Therefore, in order to better understand and define droplet transport processes in liquid spray technologies, it is necessary to systematically evaluate the factors affecting the interaction of complex transport processes in a wide range of boundary conditions.

This investigation aims to evaluate the significance of radiation absorption within a water droplet and its internal heat exchange processes, in the context of technological water spray into a flue gas flow under characteristic boundary conditions. The flue gases were treated as an air flow additionally humidified according to volumetric fraction of X_v= 0.1→0.3 and heated to a temperature T_g= 633–1833 K. In this air flow, there were no interactions between the water droplets, and the black source spectral radiation struck the droplets when T_{sour}= T_g. The convective droplet heating was defined by the initial Reynolds number Re_l< 400. The possibilities of a mechanical breakup and explosive evaporation of a droplet were ruled out, hence the cycle of consistent transformations of condensation ($\tau = 0 \rightarrow \tau_{co}$), transitional evaporation ($\tau = \tau_{co} \rightarrow \tau_e$) and equilibrium evaporation ($\tau = \tau_e \rightarrow \tau_f$) regimes were analysed:

$$\tau \equiv 0 \rightarrow \tau_{co} \rightarrow \tau_e \rightarrow \tau_f \tag{4a}$$

In the droplet phase change cycle (4a), the time moment $\tau = 0$ defines the appearance of a droplet in the gas flow and the time τ_f defines the time of droplet evaporation.

The main objectives of this research:

- To define the validity limit of the spectral radiation model [35] based on the geometric optics theory in the simulated water droplet phase change cycle (4a) based on the correspondence of the calculated absorbed radiation flux to the Harpole data [20] obtained by Mie theory;
- To improve the iterative calculation scheme based on the instantaneous balance of heat flows on the droplet surface, ensuring a consistent change of phase transformation regimes in the cycle (4a) and comprehensively taking into account the influence of the temperature of the heating droplet on the physical-spectral optical properties of water;
- To model the phase change cycle of water droplets (4a) over a wider range of flue gas temperatures, to define the role of spectral radiation absorbed in the droplet in the interaction of transfer processes in the case of complex heating, and to highlight the factors defining its specificity in the transitional regime.

2. Methodology

2.1. Problem formulation

In the regimes of phase change cycle (4a), the variation of the droplet diameter, its thermal state and vapour flux at its surface is regulars (Fig. 1a):

$$2R(\tau) \equiv 2R_0 \rightarrow 2R_{co} \rightarrow 2R_e \rightarrow 0; \tag{4b}$$

$$T_l(\tau) \equiv T_{l,0} \rightarrow T_{dp} \rightarrow T_{l,e} \rightarrow T_{l,f}; \tag{4c}$$

$$g_v(\tau) \equiv -g_{v,0} \rightarrow 0 \rightarrow g_{v,e} \rightarrow 0 \tag{4d}$$

In the condensation regime $\tau = 0 \rightarrow \tau_{co}$ the droplet warms to the dew point T_{dp} temperature, its diameter increases due to condensate and warming water expansion to $2R_{co}$, the vapour flux spreading towards the droplet, is relatively considered negative, and becomes zero at time $\tau = \tau_{co}$. In the transient evaporation regime $\tau = \tau_{co} \rightarrow \tau_e$ the droplet warms to $T_e < T_s$ temperature, its diameter decreases from $2R_{co}$ to 2_{Re} and vapour flux increases to $g_{v,e}$. In the equilibrium evaporation regime $\tau = \tau_e \rightarrow \tau_f$ the vapour flux decreases to zero and the droplet evaporates (Fig. 1a). In the case of complex heating the droplet during equilibrium evaporation cools down to T_f temperature, that is typical for the case of conductive heating. This result was achieved by modifying the droplet heating regime [37], which is ensured by reducing the slip of the droplet in the gas flow due to the effect of drag forces and by decreasing the absorption of incident radiation as the droplet shrinks during evaporation.

Assumptions made:

1. The size of a droplet is defined by the equivalent diameter of a sphere, when its volume equals to the volume of a liquid droplet;
2. There are no conditions for explosive evaporation and mechanical disintegration of the droplet;
3. The droplet transfer processes are quasi-stationary;
4. The Reynolds analogy is valid for droplet convective heating and evaporation;
5. Reynolds number for droplet is defined by the requirement Re< 400;
6. Theory of geometrical optics is valid for the droplet;
7. Spectral complex refractive index is known for the liquid.

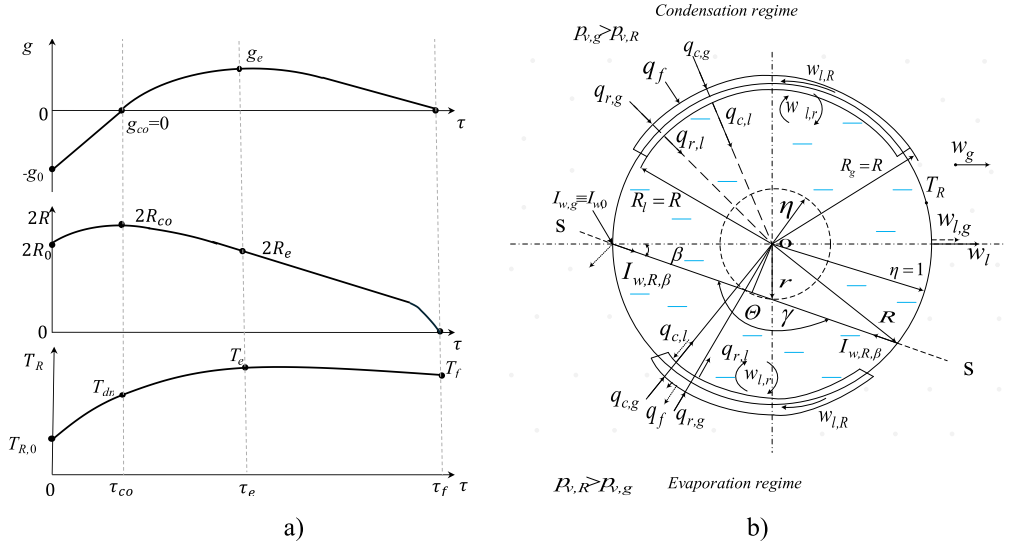

Fig. 1. Geometrical interpretations of the cycle of water droplet phase change regimes (a) and diagram of the heat fluxes on the droplet surface (b).

Then the thermal and energetic state of the droplet is related to the balance of heat fluxes flowing into and leaving the droplet's surface, which is described by the vector equation:

$$T_R(\tau) \;\leftrightarrow \vec{q}_{\Sigma,g}(\tau)+\vec{q}_{\Sigma,l}(\tau)+\vec{q}_f(\tau)=0 \;\text{, when } \vec{q}_\Sigma = \vec{q}_c+\vec{q}_r,\; \vec{q}_f = \vec{m}_v\cdot L \tag{5}$$

The Eq. (5) is transcendental and formal. Therefore, it is expected that the instantaneous temperature of the droplet surface will be calculated using an iterative method, after first transforming the Eq. (5) according to the droplet heat and mass transfer model, which must account for the possible change in the direction of the heat flux vector in the regimes of the droplet phase change cycle (4a) (Fig. 1b).

The rate of evaporation is calculated from an overall mass balance of the droplet [2,36]:

$$\begin{aligned} m_v &= \frac{g_v}{4\pi R^2};\; g_v = -\frac{4}{3}\pi\frac{d}{d\tau}\left(\rho_l R^3\right) = 2\pi R\rho_{vg}D_{vg}\overline{\mathrm{Sh}}\,\ln(1+B_M);\; \overline{\mathrm{Sh}} \\ &= 2+\frac{\mathrm{Sh}-2}{(1+B_M)^{0.7\frac{\ln(1+B_M)}{B_M}}};\; \mathrm{Sh} = 1+(1+\mathrm{Re}\,\mathrm{Sc})^{\frac{1}{3}}f(\mathrm{Re});\; B_M \\ &= \frac{Y_{v,R}-Y_{v,g}}{1-Y_{v,R}};\; Y_v = \frac{X_v}{X_vM_v+(1-X_v)M_{g,dry}};\; X_v = \frac{p_v}{p_g}. \end{aligned} \tag{6}$$

In the phase change cycle (4a) regimes are defined by dynamics of the vapour flux g_v. The condensation regime $\tau \equiv 0 \rightarrow \tau_{co}$ will occur only when water is sprayed at a temperature T_l below the dew point temperature T_{dp}, which is defined by the flue gas humidity $X_{v,g}$. The vapour flux g_v calculated by Eq. (6) is negative in the condensation regime, since the value of the Spalding mass transfer parameter B_M is negative when $Y_{v,g} > Y_{v,R}$ therefore $p_{v,g} > p_{v,R}$ (Fig. 1b). In the evaporation regime $Y_{v,R} > Y_{v,g}$, therefore $p_{v,R} > p_{v,g}$ (Fig. 1b) the calculated vapour flux g_v is positive. The condensation regime changes to the evaporation regime when $Y_{v,R} = Y_{v,g}$, therefore $g_v(\tau = \tau_{co}) = 0$ (Fig. 1a).

In the transitional evaporation regime, the droplet warms up/cools down to the thermal state characteristic to the equilibrium evaporation temperature T_e. Temperature T_e is lower than the saturation temperature T_s. Flue gas parameters define temperature T_e and are further influenced by the heating regime of the droplet. In the transitional regime the droplet warms up when $T_e/T_l > 1$ and cools down when $T_e/T_l < 1$. When the flue gas temperature T_g and humidity X_v are defined, the lowest temperature T_e will be for the droplet heated by conduction (marginal convective heating case "c"), while the highest temperature T_e will be for combined radiative-convective heating case "cr". The convective heat flux in Eq. (5) is defined from the empirical Cliff correlation, which approximate the results obtained by different authors in the range of $0.25 < (\mathrm{Pr}, \mathrm{Sc}) < 100$ and $\mathrm{Re} < 400$ with an error less than 3% [36]:

$$\begin{aligned} q_{c,g} &= \frac{\lambda_{vg}}{2R}\left(T_g-T_R\right)\cdot\left[2\frac{\ln(1+B_T)}{B_T}+\frac{\mathrm{Nu}-2}{(1+B_T)^{0.7}}\right]Nu \\ &= 1+(1+RePr)^{\frac{1}{3}}f(\mathrm{Re});\; f(\mathrm{Re}\le 1) = 1 f(1<\mathrm{Re}\le 400) = \mathrm{Re}^{0.077};\mathrm{Re} \\ &= 2R\frac{\rho_g}{\mu_{vg}}\left|w_g-w_l\right| \end{aligned} \tag{7}$$

When modelling the gas flow temperature from 633 to 1833 K, the condition $T_g > T_R$ is valid, therefore, the convective heat flux $q_{c,g}$, is described by model (7), flowing toward the droplet surface (Fig. 1b) in all regimes of the phase change cycle (4a). The influence of Stefan flow on the convective heating of an evaporating droplet is defined by the Spalding heat transfer parameter Eq. (1), taking into account the influence of the temperature gradient change in the warming droplet [29]:

$$B_T = c_{p,v,vg}\frac{T_g-T_R}{L}\left(1+\frac{q_{c,l}}{q_{c,g}}\right) = c_{p,v,vg}\frac{T_g-T_R}{L}\left[1-k_{ef}\lambda_l\frac{\partial T(r,\tau)}{\partial r}\bigg|_{r=R}\Big/ q_{c,g}\right] \tag{8}$$

In the condensation regime and during the initial stage of transitional evaporation the temperature gradient within the droplet is positive, so a convective heat flux $q_{c,l}$ flows into the droplet (Fig. 1b). However, when a temperature field with a negative gradient forms in the semi-transparent droplet due to the radiation flux absorbed within it, the vector of the $q_{c,l}$ flux reverses (Fig. 1b).

The temperature gradient variation in the droplet in the regimes of the phase change cycle (4a) is defined by model [37]:

$$\frac{\partial T(r,\tau)}{\partial r}\bigg|_{r=R} = 2\pi\sum\nolimits_{n=1}^{\infty}(-1)^n\frac{n}{R^2}\int_0^{\tau}F_{n,r}\exp\left[-\frac{k_{ef}\lambda_l}{\rho_l c_{p,l}}\left(\frac{n\pi}{R}\right)^2(\tau-\tau_*)\right]d\tau_*,$$

$$F_{n,r} = \frac{1}{R}\int_0^R (F_1+F_2)\,r\sin\frac{n\pi r}{R}\,dr;\; F_1 = \frac{1}{\rho_l c_{p,l}r^2}\frac{\partial}{\partial r}\left(r^2 q_r\right)-\frac{dT_R}{d\tau};$$

$$F_2 = \frac{1}{\rho_l c_{p,l}}\frac{\partial T_l}{\partial r}\frac{\partial\left(k_{ef}\lambda_l\right)}{\partial r}-\frac{T_l}{\rho_l c_{p,l}}\frac{\partial\left(\rho_l c_{p,l}\right)}{\partial\tau_*}. \tag{9}$$

Function $F_{n,r}$ takes into account the local radiation flux inside the droplet, the change in the surface temperature and physical properties of the water, and the influence of the water circulation. Initially, the frictional forces occurring on the surface of the sliding droplet force the liquid to flow along its surface (this flow regime is defined by the maximum liquid velocity $w_{l,R}$ [36]). Later, a vortex flow begins to form in the droplet, which is conditionally defined by the velocity $w_{l,r}$ (Fig. 1b). The influence of circulation on the convective heat flux $q_{c,l}$ in the droplet is evaluated using the effective thermal conductivity parameter, which is calculated according to Eq. (3).

The intensity of spectral radiation falling on an individual droplet is equated to blackbody radiation (it is believed that this is ensured by the radiation of soot-covered surfaces and multiple light reflections in the droplet ensemble). In the case of spectral absorption, the behaviour of a semitransparent spherical droplet is explained using geometric optics, and the change in spectral radiation intensity in the S direction is defined as the change in the direction of the spherical droplet radius R (Fig. 1b):

$$\begin{aligned} &\frac{\mathrm{d}I_\omega}{\mathrm{d}s} = \pm\frac{\left(r^2-R^2\sin^2\beta\right)^{1/2}}{r}\frac{\mathrm{d}I_\omega}{\mathrm{d}r}, \\ &\text{where } \;''-''\; \text{as } \; 0\le s< R\cos\beta;\;\; ''+''\; \text{as } \; R\cos\beta\le s< 2R\cos\beta. \end{aligned} \tag{10}$$

Then the local radiation flux in the water droplet is described by the model [35]:

$$q_r(r) = 2\pi\int_0^{\infty}\int_0^{\pi/2}\sin\gamma\cos\gamma\left(I_{\omega,1}+I_{\omega,2}-I_{\omega,3}-I_{\omega,4}-I_{\omega,5}\right)d\gamma d\omega. \tag{10a}$$

$$I_{\omega,1} = I_{\omega,R,\gamma}\exp\left(-\xi_r^R\right);\; I_{\omega,2} = \int_r^R n_{\omega,l}^2 I_{\omega,0}3\exp\left(-\xi_r^{r_*}\right)d\xi_r^{r_*};$$

$$I_{\omega,3} = I_{\omega,R,\gamma}\exp\left(-\xi_{r\sin\gamma}^R-\xi_{r\sin\gamma}^r\right);\; I_{\omega,4} = \int_{r\sin\gamma}^r n_{\omega,l}^2 I_{\omega,0}\exp\left(-\xi_{r_*}^r\right)d\xi_{r_*}^r;$$

$$I_{\omega,5} = \int_{r\sin\gamma}^{R} n_{\omega,l}^2 I_{\omega,0} \exp\left(-\xi_{r\sin\gamma}^{r} - \xi_{r\sin\gamma}^{r_*} \right) d\xi_r^{r_*}. \tag{11}$$

$$I_{\omega,R,\gamma} = \frac{\left(1-\kappa_{\omega,\beta}\right) n_{\omega,l}^2 I_{\omega 0}\left(T_g\right) + \kappa_{\omega,\beta} \int_{R\sin\gamma}^{R} n_{\omega,l}^2 I_{\omega,0} \left[\exp\left(-\xi_{R\sin\gamma}^{R} - \xi_{R\sin\gamma}^{r_*} \right) + \exp\left(-\xi_{r_*}^{R} \right) \right] d\xi_R^{r_*}}{1-\kappa_{\omega,\beta}\exp\left(-2\tau_{R\sin\gamma}^{R} \right)}; \tag{12}$$

$$\xi_{r_1}^{r_2} = \int_{r_1}^{r_2} d\xi_{r_1}^{r_2} = \int_{r_1}^{r_2} \frac{\chi_\omega dr_*}{\sqrt{1-(r/r_*)^2 \sin^2\gamma}}; \gamma = \pi - \theta; R\sin\beta = r\sin\gamma; \tag{13}$$

$$I_{\omega 0} = 2C_0^2 \omega^3 C_1 \left\{ \exp\left[\frac{C_0 \omega C_1}{C_2 T(\psi,\Theta)} \right] - 1 \right\}^{-1}; \overline{n}_\omega = n_\omega - ik_\omega; \chi_\omega = 4\pi k_\omega \omega. \tag{14}$$

In the Planck function expression (14), $C_0 = 2.9979 \cdot 10^8$, m/s; $C_1 = 6.6256 \cdot 10^{-34}$, J s; $C_2 = 1.38054 \cdot 10^{-23}$, J/K. In the formal expression of the optical thickness (13), the radial coordinates r_1 and r_2 represent indices of integrals in Eqs. (11, 12). A light beam with intensity $I_{\omega,\psi}$ and falling from the outside at an angle ψ is partially reflected by droplet surface and propagates in the droplet at an angle β. From the internal side, a light beam that falls at angle β is partially reflected (the other part refracts and leaves the droplet in the direction of the angle ψ) and strengthens the light beam intensity inside the droplet. The spectral radiation model presented takes into account the water spectral radiation, the radiation absorption into water, and the impact of the Brewster angle:

$$\beta_{\omega,\max} = \arcsin\left(\frac{\overline{n}_{\omega,g}}{\overline{n}_{\omega,l}} \right) \tag{15}$$

The spectral reflection coefficient $\kappa_{\omega,\beta}$ is described according to the model of polarised light [18]:

$$\begin{aligned} \kappa_{\omega,\beta} = \kappa_{\omega,\psi} &= \frac{1}{2}\left(r_{\omega\perp,\psi} + r_{\omega//,\psi} \right); \kappa_{\omega\perp,\psi} \\ &= \frac{\left(n_{\omega,l}\cos\beta - n_{\omega,g}\cos\psi \right)^2 + \left(k_{\omega,l}\cos\beta - k_{\omega,g}\cos\psi \right)^2}{\left(n_{\omega,l}\cos\beta + n_{\omega,g}\cos\psi \right)^2 + \left(k_{\omega,l}\cos\beta + k_{\omega,g}\cos\psi \right)^2} \kappa_{\omega//,\psi} \\ &= \frac{\left(n_{\omega,l}\cos\psi - n_{\omega,g}\cos\beta \right)^2 + \left(k_{\omega,l}\cos\psi - k_{\omega,g}\cos\beta \right)^2}{\left(n_{\omega,l}\cos\psi + n_{\omega,g}\cos\beta \right)^2 + \left(k_{\omega,l}\cos\psi + k_{\omega,g}\cos\beta \right)^2}. < \text{mmEquation id} \\ &= ''\text{eqn3}'' \quad / > \end{aligned} \tag{16}$$

The complex spectral index of refraction for water is defined according to [32,33] data.

The presented model of the heat fluxes of the evaporating droplet in the case of complex radiative-convective-radiative heating is universal for phase change cycle (4a) regimes. Therefore, the formal heat flow balance Eq. (5) is presented in a form suitable for numerical calculations:

$$T_R(\tau) \leftrightarrow \lambda_{vg} \frac{\mathrm{Nu}_f}{2R} \left(T_g - T_R \right) + \left(q_{r,g} - q_{r,l} \right) - k_{ef}\lambda_l \left. \frac{\partial T(r,\tau)}{\partial r} \right|_{r=R} - \frac{g_v}{4\pi R^2} L \tag{17}$$

The droplet thermal state is defined according to its instantaneous mass mean temperature:

$$T_m = \frac{\int_o^R \rho_l \, c_{p,l} \, T_l(r,\tau) \, r^3 dr}{\int_o^R \rho_l \, c_{p,l} \, r^3 dr}. \tag{18}$$

In Eq. (18), the temperature field in the droplet is described according to [37] model:

$$T(r,\tau) = T_R(\tau) + \frac{2}{r} \sum_{n=1}^{\infty} \sin\frac{n\pi r}{R} \int_0^\tau F_{n,r} \exp\left[-\frac{k_{ef}\lambda_l}{\rho_l c_{p,l}} \left(\frac{n\pi}{R} \right)^2 (\tau - \tau_*) \right] d\tau_*. \tag{19}$$

Expression (19) is used to define the local temperature gradient in the droplet:

$$\begin{aligned} \frac{\partial T(r,\tau)}{\partial r} = 2 \sum_{n=1}^{\infty} &\left(\frac{n\pi}{r\,R} \cos\frac{n\pi r}{R} - \frac{1}{r^2} \sin\frac{n\pi r}{R} \right) \int_0^\tau F_{n,r} \exp \\ &\left[-\frac{k_{ef}\lambda_l}{\rho_l c_{p,l}} \left(\frac{n\pi}{R} \right)^2 (\tau - \tau_*) \right] d\tau_*. \end{aligned} \tag{20}$$

2.2. Method of solution

The phase change of the water droplet is modelled using QBASIC with the original numerical modelling programme "LASAS", when the numerical iterative scheme defining the average instantaneous temperature T_R of the droplet surface works according to the fastest descent method and is based on Eq. (17). The dimensionless radial coordinate $\eta = r/R$ is used, which in the cycle (4a) ensures the unit dimensionless radius $\eta = 1$, when $r = R$. Then, the linear grid in the range $\eta = 0 \rightarrow 1$, defining the local 41 [47] cross-sections inside the droplet, are marked, remains unchanged throughout the entire cycle of droplet phase changes:

$$\eta_1 = 0; \Delta\eta = \frac{1}{J-1}; \eta_{j>2} = \eta_{j-1} + \Delta\eta; \sum_{j=2}^{J} \left(\eta_j - \eta_{j-1} \right) = 1 \tag{21}$$

The time step ΔFo in the cycle of phase change regimes (4a) is defined on the Fourier scale for the selected flue gas temperatures T_g. This allows for the individual time coordinate grid to be calibrated for droplets of different dispersity according to the universal ΔFo of each T_g.

$$\tau_1 = 0; \tau_{i>1} = \tau_{i-1} + \Delta\tau; \sum_{i=2}^{I_f} \left(\tau_i - \tau_{i-1} \right) = \tau_f. \tag{22}$$

The water droplet evaporation time τ_f depends on the flue gas temperature, the droplet size and the method of heating (Fig. 2a, c). Therefore, the time step for each investigated case is individual. It is not convenient to perform a numerical investigation over a wide range of boundary conditions. Therefore, the impact of the droplet size on temperature T_g is partially eliminated by using the Fourier time scale $\mathrm{Fo} = \left(a_{l,0}/R_0^2 \right) \tau$. The convective heating case "c" is defined by the Re_0 number, while the droplet evaporation dynamics is only influenced by air flow temperature T_g, which is confirmed by the overlapping dotted lines (Fig. 2b, d).

At each time moment τ_i, starting from τ_2, the iterative $it \equiv 1 \rightarrow IT$ calculations are performed to define the instantaneous droplet surface temperature $T_{R,i}$. For the first iteration $it = 1$, the temperature $T_{R,i-1}$ is already defined, while the temperature $T_{R,i.it}$ for other iterations is provided by the software "LASAS". In each iterative calculation, temperature $T_{R,i} = T_{R,i,IT}$ is being defined, where:

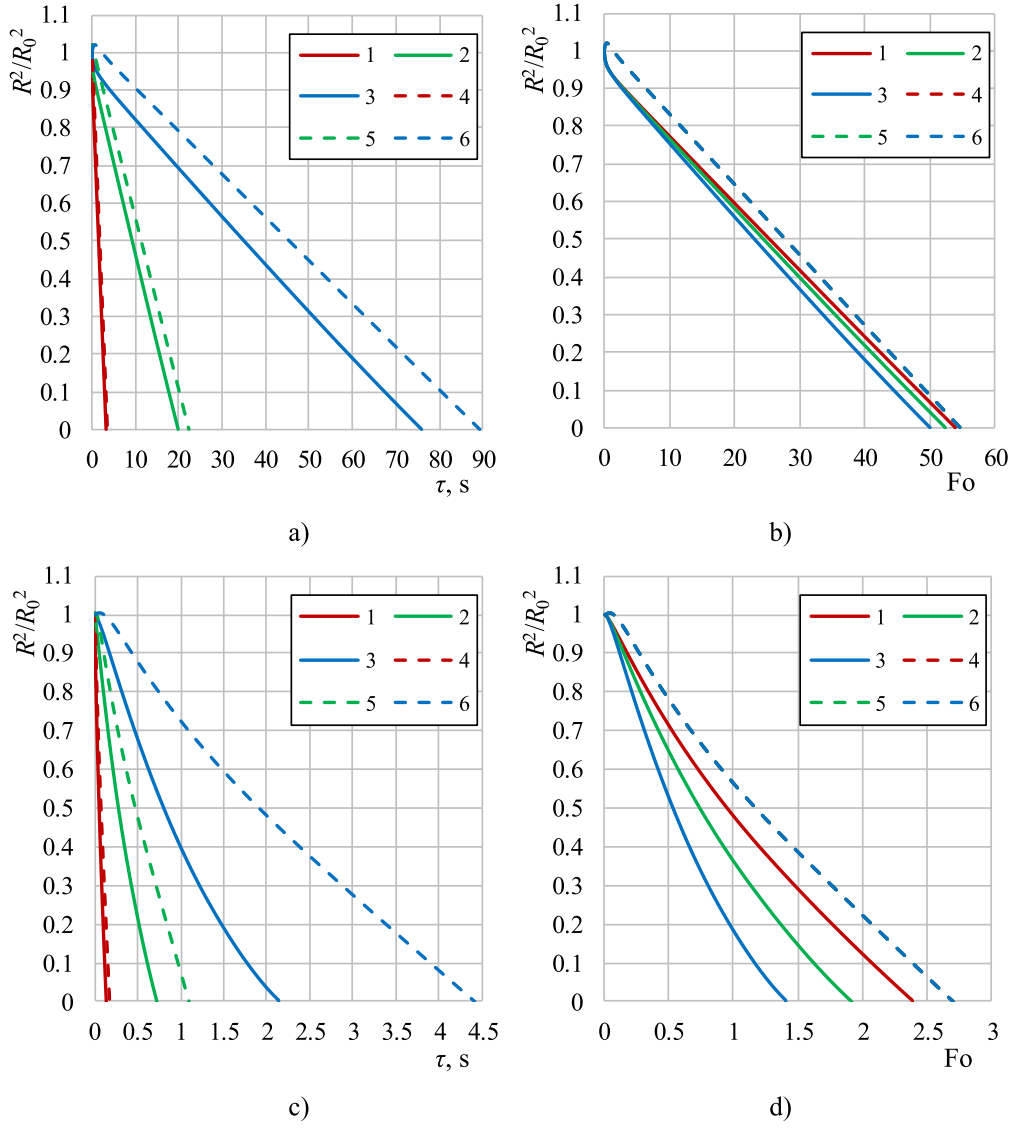

Fig. 2. Time history of the dimensionless surface area R^2/R_0^2 of water droplets during their evaporation at 450 K (a, b) and 1550 K (c, d) temperature air in the cases of combined "cr" (solid lines) and convective "c" (dotted lines) heating in the real time scale (a, c) and in the Fourier number scale (b, d). $2R_0$, μm: (1,4) 200, (2,5) 500, (3,6), 1000. $\mathrm{Re}_0 = 10$; $T_{sour} = T_g$; $\varepsilon_{sour} = 1$.

$$\delta_{IT} = \left|1 - \frac{q_{c,l,i,IT} + q_{f,i,IT}}{q_{c,l,i,IT}}\right| \times 100\% < 0.05\%. \tag{23}$$

Only when the instantaneous droplet radius $R_{I,it}$ is defined can the ordinary iteration it be performed in iterative $it{=}1{\to}IT$ calculations. Therefore, an assumption $R_{I,it=1}{=}R_{I-1}$ is made for the first iteration. For the next iterations, it is assumed that $R_{I,it>1}{=}R_{I,it-1}$. The instantaneous droplet radius is adjusted after each iteration it:

$$R_{I,it}^3 = R_{I-1}^3 - \frac{R_{I-1}^2 + R_{I,it-1}^2}{\rho_{l,m,I-1} + \rho_{l,m,I,it}} \left(3\frac{m_{v,I-1}^+ + m_{v,I,it}^+}{2} + \frac{R_{I-1} + R_{I,it-1}}{4}\frac{\rho_{l,m,I,it} - \rho_{l,m,I-1}}{\tau_i - \tau_{i-1}}\right)(\tau_i - \tau_{i-1}). \tag{24}$$

For selected instantaneous droplet surface temperatures $T_{R,i,it}$, the temperature field in the droplet and its gradient are calculated numerically according to the schemes:

$$T_{j,i} = T_{J,I} + \frac{2}{\eta_j R_I}\sum_{n=1}^{\infty}\sin(n\pi\eta_j)\sum_{i=2}^{I}\bar{f}_{n,i,it}\bar{f}_{n,i,\tau}, \text{when} I = 2{\to}(I_f - 1); \tag{25a}$$

$$\left.\frac{\partial T_{j,i}}{\partial r}\right|_{r=R_I} = \frac{2\pi}{R_I^2}\sum_{n=1}^{\infty}(-1)^n n\sum_{i=2}^{I}\bar{f}_{n,i,it}\bar{f}_{n,i,\tau}, \text{when} I = 2{\to}(I_f - 1). \tag{25b}$$

Functions f_n are defined according to numerical schemes [37]:

$$\bar{f}_{n,i,\tau} = \int_{\tau_{i-1}}^{\tau_i}\exp\left[-a_{l,ef,i}\left(\frac{n\pi}{R_i}\right)^2(\tau_I - \tau)\right]d\tau = \frac{1}{\bar{a}_{l,ef,i}}\frac{\bar{R}_i^2}{n\pi}\left\{\exp\left[a_{l,ef,i}\left(\frac{n\pi}{R_i}\right)^2(\tau_I - \tau_i) - \exp\left[a_{l,ef,i-1}\left(\frac{n\pi}{R_{i-1}}\right)^2(\tau_I - \tau_{i-1})\right]\right]\right\}; \tag{26a}$$

$$\bar{f}_{n,i,\eta} = \sum_{j=2}^{J} \frac{1}{\bar{\rho}_{l,j,i}\bar{c}_{p,l,j,i}} \int_{\eta_{j-1}}^{\eta_j} \frac{1}{i\eta} \frac{d(\eta^2 \bar{q}_{r,i,\eta})}{d\eta} \sin n\pi\eta d\eta$$

$$+ \sum_{j=2}^{J} \frac{1}{\bar{\rho}_{l,j,i}\bar{c}_{p,l,j,i}} \left(\frac{1}{\bar{R}_i} \frac{\bar{T}_{l,j,i} - \bar{T}_{l,j-1,i}}{\eta_j - \eta_{j-1}} \frac{\bar{\lambda}_{l,j,i} - \bar{\lambda}_{l,j-1,i}}{\eta_j - \eta_{j-1}} \right.$$

$$\left. - \bar{R}_i \bar{T}_{l,j,i} \frac{\rho_{l,j,i} c_{p,l,j,i} - \rho_{l,j,i-1} c_{p,l,j,i-1}}{\tau_i - \tau_{i-1}} \right) \int_{\eta_{j-1}}^{\eta_j} \eta \sin n\pi\eta \, d\eta$$

$$- \bar{R}_i \sum_{j=2}^{J} \frac{T_{J,i} - T_{J,i-1}}{\tau_i - \tau_{i-1}} \int_{\eta_{j-1}}^{\eta_j} \eta \sin n\pi\eta \, d\eta; \quad (26b)$$

$$\bar{R}_i = \frac{R_{i,it-1} + R_{i-1}}{2}; \bar{a}_{l,ef,i} = \frac{a_{l,ef,j,i} + a_{l,ef,j-1,i}}{2}; \bar{q}_{r,i,\eta} = \frac{q_{r,i,\eta} + q_{r,i-1,\eta}}{2};$$

$$\bar{\rho}_{l,j,i} = \frac{\rho_{l,j,i,it-1} + \rho_{l,j,i-1}}{2}; \bar{c}_{p,l,j,i} = \frac{c_{p,l,j,i,it-1} - 1 + c_{p,l,j,i-1}}{2};$$

$$\bar{T}_{l,j,i} = \frac{T_{l,j,i,it-1} + T_{l,j,i-1}}{2}; \bar{T}_{l,j-1,i} = \frac{T_{l,j-1,i,it-1} + T_{l,j-1,i-1}}{2};$$

$$\bar{\lambda}_{l,j,i} = \frac{\lambda_{l,j,i,it-1} + \lambda_{l,j,i-1}}{2}; \bar{\lambda}_{l,j-1,i} = \frac{\lambda_{l,j-1,i,it-1} + \lambda_{l,j-1,i-1}}{2} \quad (26c)$$

In numerical scheme (26b), the radial coordinate η integrals are solved when integrating by parts. In the iteration *it*, the local radiation flux $q_{r,j,i,it}$ in a droplet at time τ_i is calculated according to the temperatures field $T_{j,i,it-1}$ that has been made more precise in earlier iteration. In the local radiation flux expression (10a), the integral of the wave number is calculated numerically using rectangular method dividing the radiative spectrum ω=50→12500 cm^{-1} uniformly into 157 sections according to the recommendations in [20]. The integral of angle γ in expression (10a) is calculated numerically using the Gaussian method

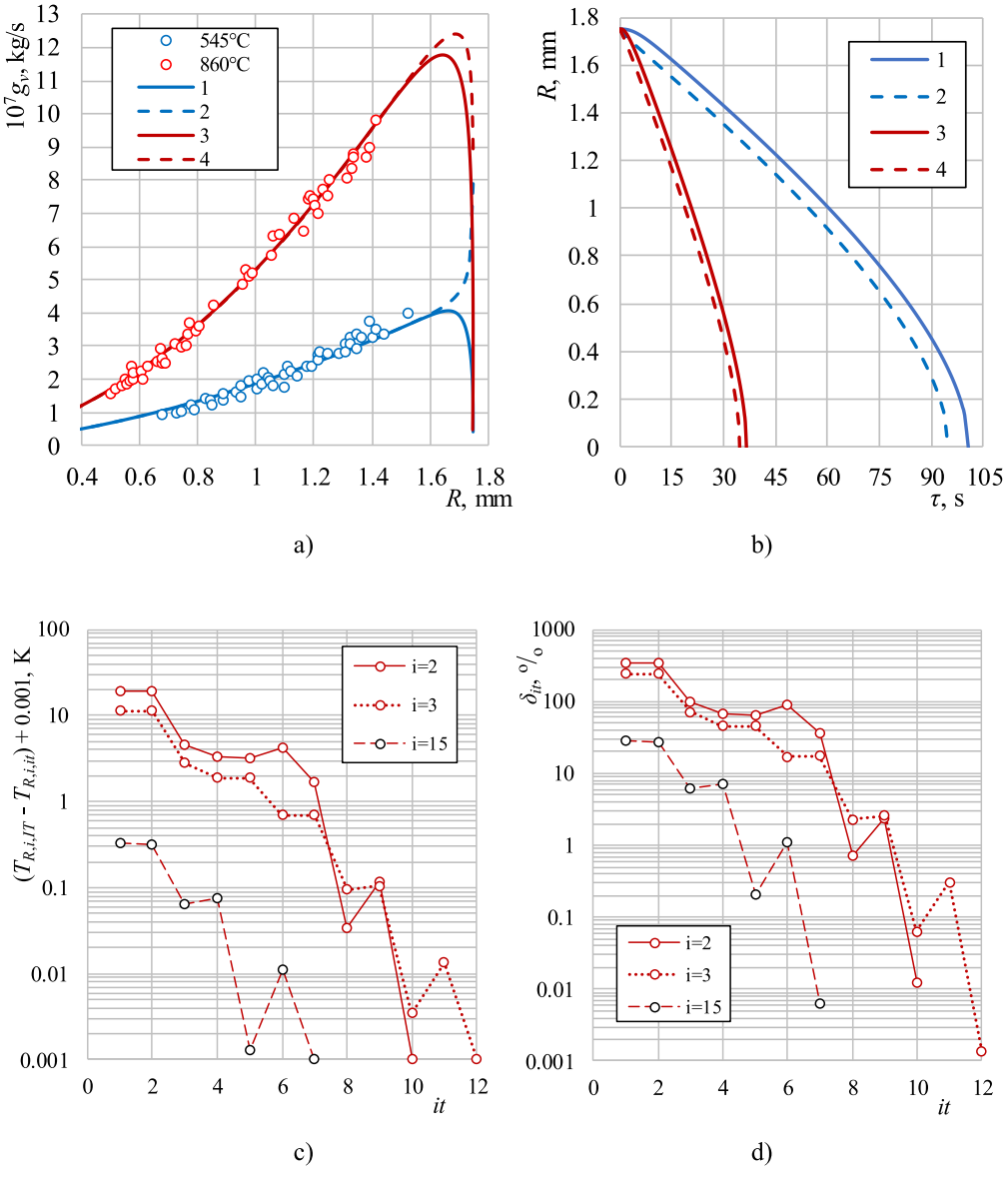

Fig. 3. The dependence of vapour flux on the water droplet size (a) and time history of droplet evaporation (b) in the case of radiative-convective heating, and examples of the iterative calculations of the instantaneous $T_{R,i}$ temperature (c) and with its the accompanying relative instantaneous disbalance between the heat fluxes (d). Points – experiment data [45]; Lines – present model, when T_g, K: (1,2) 818, (3,4) 1133; $T_{l,0}$, K: (1,3) 313, (2,4) 363; $X_{v,g}$= 0.01; w_g= 0.01 m/s; $2R_0$ = 3.5 mm; w_l= 0; ε_w= 0.9; T_{sour}= T_g, $\tau_{i=2}$ = 0.0114 s; $\tau_{i=2}$ = 0.0228 s; $\tau_{i=2}$ = 0.16 s. In Fig. 2a: δ_e= (1-$g_{v,e,IT}$ /$g_{v,eks}$)·100 °/$_o$= (0→3.9) °/$_o$.

according to a 9-point scheme, which allows evaluation of precisely the influence of the Brewster angle on the local radiative flux in the droplet. The subintegral function in expression (10a) is determined by recommendations in [35], when in the most common case optical thickness in Eqs. (11–13) are calculated as:

$$\xi^{r_j}_{r\sin\gamma} = \xi^{r_{j0}}_{r\sin\gamma} + \xi^{r_j}_{j0} = \chi_{\omega,j0}\sqrt{r_{j0}^2 - r^2\sin^2\gamma} + \sum_{jj=j0}^{j-1}\chi_{\omega,jj}\left(\sqrt{r_{j0}^2 - r^2\sin^2\gamma} - \sqrt{r_{jj}^2 - r^2\sin^2\gamma}\right), \quad (27)$$

under the validity of condition that $r_{j0-1} < r\sin\gamma \le r_{j0}$.

Figs. 3c and 3d present examples of iterative calculations of the instantaneous temperature of the droplet's surface and the accompanying relative instantaneous disbalance between the heat fluxes.

At relatively low air flow temperatures, the impact of an additional radiation flux on the droplet evaporation dynamics is not significant (Fig. 2b); however, at high temperature cases, the effect of radiation is more significant for larger droplets (Fig. 2d). Therefore, in the performed numerical investigation for the average droplet diameter of $2R = 500$ μm, the optimal Fourier variation steps ΔFo≡0.1; 0.06; 0.02; 0.008; 0.004 and 0.001 were defined when gas Tg [K] temperature was 433; 633; 933, 1233, 1533 and 1833, respectively. For intermediate temperatures T_g, intermediate ΔFo steps were selected. In the case of the individual investigation, the time step $\Delta\tau$ for a droplet size of $2R_0$ is defined based on ΔFo in the phase change cycle (4a):

$$\Delta\tau = \frac{R_0^2}{a_0}\,\Delta\mathrm{Fo}\,. \quad (28)$$

Iterative calculations at the time $\tau_{i=If}$ are not possible. Therefore, the droplet evaporation time τ_f is defined geometrically based on the individual evaporation curve in Fig. 2. It is important to emphasise that an iterative calculation for the condensation regime and its change to the evaporation regime may not converge at the time close to the end of condensation regime. Hence, at the beginning, it is necessary to model the initial stage of the droplet phase change cycle (4a) and, if necessary, to adjust time step Δτ minimally to ensure a smooth change in the phase regime change from condensation to evaporation.

The dimensionless time scale t/t_f is used for comparative analysis of simulation results under different boundary conditions.

2.3. Model validation

To verify the water droplet evaporation model, Fig. 3a compares the droplet evaporation rate g_v predicted by the present model with experimental data reported by Ivanov and Smirnova [45]. Similarly, Fig. 4 compares the absorbed radiation flux in water droplets predicted by the model (10−16) with modelling results by Harpole [20].

Droplet evaporation dynamics depend on the temperature of the environment, and, in the case of a hot water droplet, it evaporates faster (Fig. 3b). The functional dependence of the vapour flux $g_{v,i}(R)$ on the instantaneous water droplet diameter $2R_i$ is shown in Fig. 3a. The vapour flux of a warm 313 K temperature water droplet increases in the transitional evaporation regime (Fig. 3a solid lines), irrespective of the air temperature. Meanwhile, in the case of a hot (363 K) water droplet, the vapour flux $g_{v,i}$ increases in the 1133 K temperature air (Fig. 3a line 4), and decreases in the 818 K temperature air (Fig. 3a line 2). Plots 1 and 2 show the opposite behaviour at the radius of 1.8 mm (Fig. 3a). This is defined by the dimensionless parameter T_e/T_l of the initial temperature of the droplet. When $T_e/T_l > 1$ (cases 1, 3 and 4), the evaporation rate is initially low, since the heat supplied to the droplet heats it intensively. In these cases, the evaporation rate of the droplet increases in the transitional regime up to the equilibrium evaporation rate. When $T_e/T_l < 1$ (case 2), the evaporation rate is initially high, since the evaporation process additionally involves a heat flux proportional to the change in the enthalpy of the cooling droplet. Therefore, in case (2), the evaporation rate of the droplet in the transitional regime decreases to the equilibrium evaporation rate. In all (1−4) cases, the evaporation rate decreases in the equilibrium regime, since the droplet decreases, and the absorption of radiation in it weakens.

In the equilibrium evaporation regime the vapour flux $g_{v,i}$ decreases consistently in all cases and agrees well with the experimental data (Fig. 3a). Since the convective heating conditions do not change much during the evaporation of the droplet, the essential impact of absorbed radiation on vapour flux dynamics can be foreseen. Its definition requires a more detailed assessment, which is provided in Section 3.1.

Fig. 4 shows the absorbed thermal radiative flux calculated from model (2) in a water droplet, with the effective absorption α_{ef} chosen from Table 1 of [20]. The calculated water droplet radiative flux q_r [kW/m^2] absorbed inside a water droplet that is based on the geometrical optics model (10−16) in a wide temperature T_g≡450→1450 K range and a wide droplet size variation $2R$≡20→2000 μm range is in good agreement with the Harpole modelling results based on Mie theory. The slight difference between the present results and those of

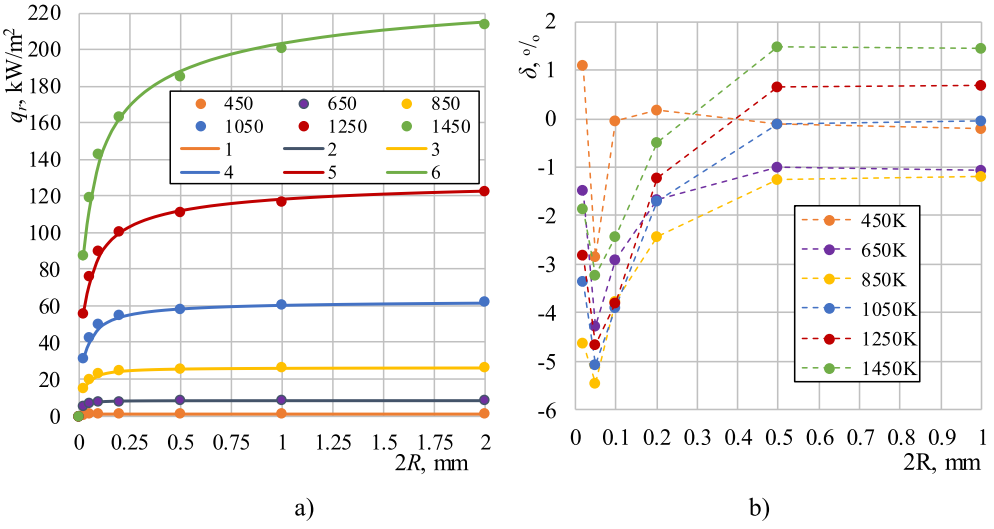

Fig. 4. Absorbed radiation flux in water droplet(a) and relative error of its calculation (b). Points (a) – Modelling results for Harpole Mie theory [20]; Solid lines – present model, when T_g, K: (1) 450, (2) 650; (3) 850, (4) 1050; (5) 1250, (6) 1450; $T_{l,0} = 373$ K; $\varepsilon_{sour} = 1$; $T_{sour} = T_g$.

Harpole can be related with the uneven evaluation of the dependence of the spectral complex's refractive index on water temperature.

The relative error (δ) of the radiation flux absorbed by a water droplet, calculated using the geometrical optics model overt the black-body temperature range 450→1450 K, does not exceed 2% for large droplets 2 R > 200 μm. For medium-sized droplets, 2 R = 200→20 μm, δ < 5.5% (Fig. 4b) when compared with Harpole's Mie-theory data. Therefore, in this study, the limit of applicability of the geometric optics model is defined by the condition 2 $R\geq$ 20 μm. The local radiative flux in the water droplet in the cycle (4a) is calculated according to the geometrical optics-based model (10−16) for droplets, for which the diameter is larger than 20 μm. In the last stage of evaporation, the droplet diameter decreases rapidly, and the radiation absorption is assumed to be linearly attenuated to zero.

3. Results

The role of radiation is defined by a comparative assessment of phase change cycle (4a) modelling results of droplet combined "cr" and convective "c" heating cases. In the convective heating case "c", T_{sour}= 0. The numerical investigation was performed in two stages. In the first stage, the radiation impact for the thermal state of water droplets and phase changes were investigated when the convective component of external heating is weak and close to the conductive heating case but still allowed to rule out the influence of self-contained convection. In the second stage, the impact of water forced circulation

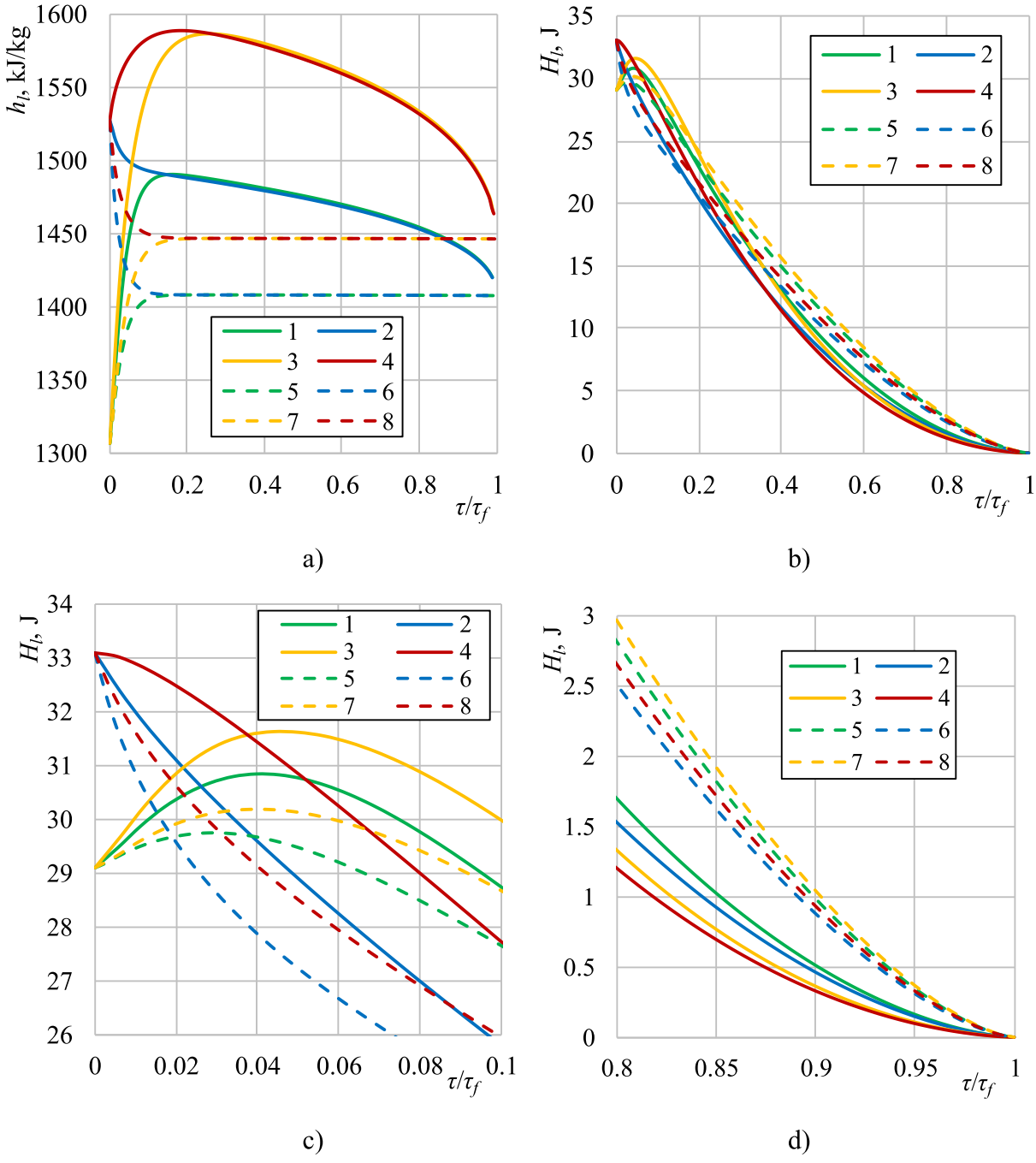

Fig. 5. Time history of the enthalpy of a droplet h_l (a) and H_l (b,c,d) in the cases of combined "cr" (solid lines) and convective "c" (dotted lines) heating. T_g, K: (1,2,5,6) 818, (3,4,7,8) 1133; $T_{l,0}$, K: (1,3,5,7) 313, (2,4,6,8) 363; $X_{v,g}$= 0.01; w_g= 0.01 m/s; $2R_0$ = 3.5 mm; w_l= 0; ε_w= 0.9; T_{sour}= T_g.

arising due to droplet slipping was evaluated.

3.1. The role of thermal radiation absorption

In this investigation, under weak external convection, an additional condition was introduced that any increase of friction forces on the slipping droplet surface would be insufficient to introduce forced water circulation inside the droplet. According to the convective heat transfer model in the droplet in the Spalding heat parameter Eq. (7), the condition is ensured by the $ke_f(\mathrm{Pe}_l<2.5)\approx 1$. For model validation cases the requirement $\mathrm{Pe}_l< 2.5$ was ensured.

Peculiarities of the droplet's thermal and energy state variation are clearly illustrated by its enthalpy change during the phase change cycle (4a) (Fig. 5). The variation of enthalpy (Fig. 5a) defines the averaged droplet mass temperature function $T_{l,m}(\tau)$ qualitatively. Full enthalpy H_l variation (Fig. 5b) directly describes droplet energy state dynamics and is related with droplet mass change caused by phase changes. When the equivalent diameter of the droplets is the same, the initial difference in mass is determined only by the density of water at different temperatures. Flue gas temperature and way of droplet heating have a pronounced effect on the enthalpy dynamics in the initial stage of droplet evaporation (Fig. 5c). By the end of evaporation, the enthalpy H_l exhibits nearly the same behaviour in all cases (Fig. 5d). In the equilibrium evaporation regime, the overlapping curves 1 and 2; 3 and 4; 5 and 6; 7 and 8 justify that the initial temperature of water $T_{l,0}$ does not have an impact on this phase change regime (Fig. 5a). However, the grouping of the overlapping curves not only with air temperatures of 818 K and 1133 K, but also with heating cases "c" and "cr" confirms the importance of these factors. In the case of weak external convective heating "c" due to air temperature changes in all modelled cases, the droplet enthalpy h_l increases from 1408 kJ/kg to 1446 kJ/kg.

In the case of complex heating "cr", the most significant increase in enthalpy h_l can be observed at the beginning of the equilibrium evaporation from ≈ 1490 kJ/kg to ≈ 1590 kJ/kg, therefore the higher temperature of the radiation source caused the increase in the droplet enthalpy by ≈ 64 kJ/kg (Fig. 5a). In the transitional phase change regime, the influence of the initial water temperature is essential and not only causes the specific droplet enthalpy dynamics (Fig. 5) but also leads to a specific variation of non-isothermal of a droplet (Fig. 6a) and its temperature gradient (Fig. 6b). Solid lines of grad$T$ in Fig. 6b converge to zero at the final stage of droplet evaporation. The droplet cools at 363 K, meaning that the grad$T$ is negative from the start. The droplet

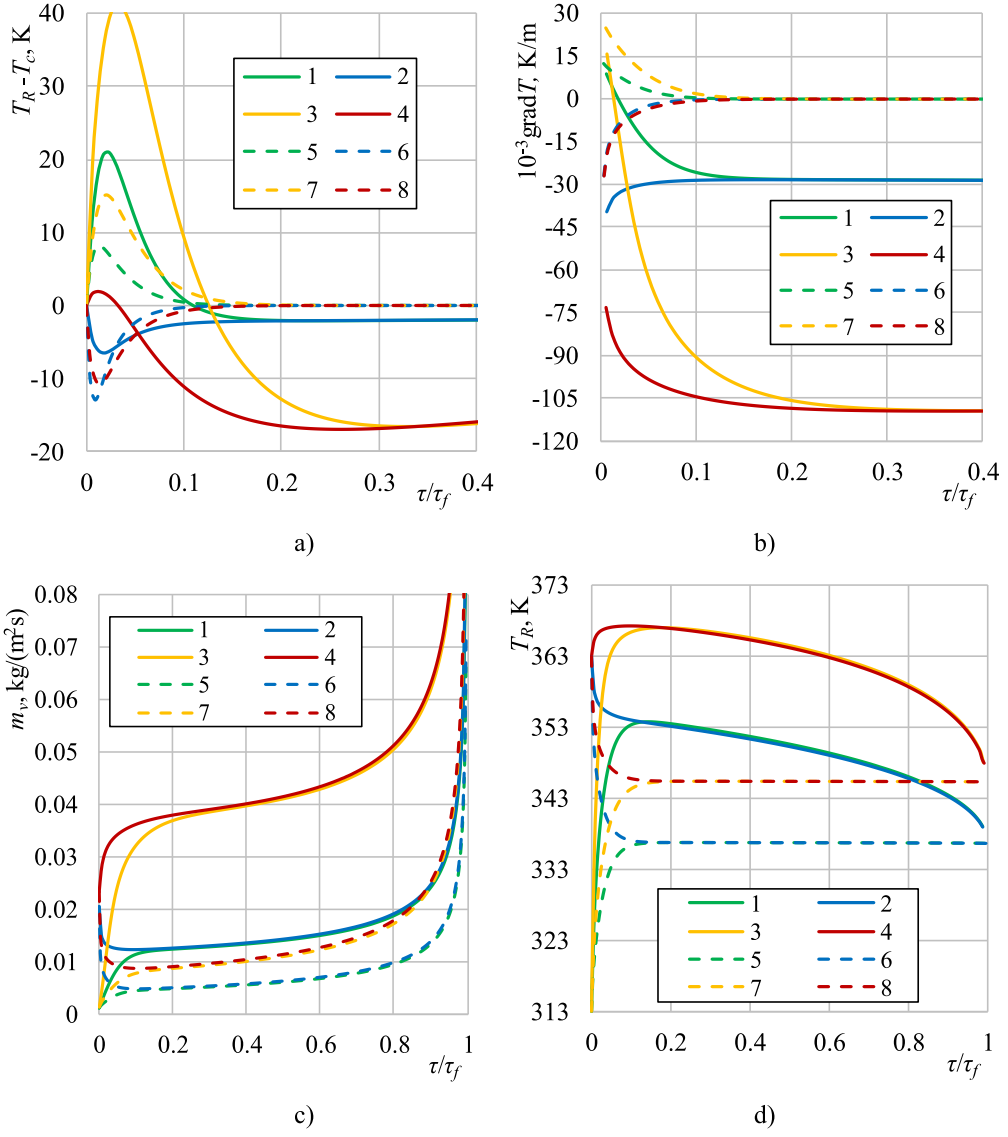

Fig. 6. Time history of temperature difference T_R-T_c of a droplet (a), its temperature gradient (b), vapour flux density (c) and droplet surface temperature T_R (c). Markings as in Fig. 5.

warms at 313 K, meaning that the grad$T$ is initially positive and becomes negative due to the effect of absorbed radiation, when the inner layers of the droplet heat up to a higher temperature than its surface. The opposite behaviour of plot 1 and 2, shown in Fig. 6a, is determined by the specific of T_e/T_l parameter: in case 1, $T_e/T_l > 1$, and thus the droplet warms up and its surface temperature increases faster than the core temperature; in case 2, $T_e/T_l < 1$, the droplet cools and its surface temperature decreases faster than the core temperature. Plot 3 is significantly higher than plot 4, since the initial droplet temperature 313 K is significantly lower than the equilibrium evaporation temperature T_e. In case 4, the initial temperature 363 K is close to T_e, so the droplet rapidly warms up to the thermal state characteristic to the equilibrium evaporation. The intensity of phase changes in the cycle (4a) is determined by the dynamics of vapour flux density (Fig. 6c), which is defined by the change in the droplet surface temperature (Fig. 6d). The droplet surface temperature variation, as well as phase change dynamics is defined not only by the temperature of the air flow but also by the radiation source temperature, water temperature, and droplet heating process. In the modelled cases, the initial water temperature $T_{l,0}$ is higher than the dew point temperature T_{dp}, defined by the low humidity air, and therefore, the condensation regime is absent, and the calculated vapour flux is positive (Fig. 6c).

In the transitional evaporation regime, the droplet warms up to the equilibrium evaporation temperature T_e. In the case of convective heating "c", the temperature T_e is 336.8 K and 345.4 K, when T_g is 818 K and 1133 K, respectively (Fig. 6d). A water droplet of 313 K temperature warms up to T_e, while a water droplet of temperature 363 K cools down towards T_e (Fig. 6d dotted lines). In the combined heating case "cr", the temperature T_e rises to 353.8 K and 366.9 K, respectively due to the impact of the radiation flux. In this case, the water droplet of 313 K temperature also warms up to temperature T_e. Interestingly, in the "cr" case, the water droplet of 363 K in the air flow of T_g 1133 K warms up to T_e (Fig. 6d 4 line), while in the T_g 818 K it cools down to T_e (Fig. 6d 2 line). This shows that the droplet's thermal state dynamics could not be unambiguously predicted according to the sensory water temperature because droplet heating processes and equilibrium evaporation temperature need to be additionally taken into account.

In a semi-transparent liquid, the radiation impact on combined heat transfer processes is clearly demonstrated by the non-isothermal droplet and in its temperature gradient dynamics. In the case of weak convection ("c" case), due to the rapid warming / cooling of the surface layers at the initial stage, the first non-isothermal peak forms inside the droplet (it could reach up to ±15 K), which disappears during the transitional evaporation (Fig. 6a dotted lines). However, in the combined heating case "cr", the first non-isothermal maximum can exceed 40 K, then drop to zero. Later, due to the radiation impact, the second non-isothermal maximum forms, which can exceed 15 K in 1133 K temperature air (Fig. 6a solid lines). It is important to notice that the absorbed radiation flux allows a negative temperature gradient to form (Fig. 6b 1,3,5,7 lines) in water droplets at the 313 K temperature. In 363 K temperature water droplets, a negative temperature field gradient form immediately (Fig. 6b 1,3,5,7 lines), and the absorbed radiation flux slows down the cooling of the inner droplet layers. In the 818 K temperature air, the evaporation in a large droplet intensifies by more than two times due to the influence of radiation, while in the 1133 K air it is up to 4 times (Fig. 6c).

3.2. The role of droplet slipping and gas temperature

The movement of sprayed water droplets in a gas flow is influenced by gas flow parameters such as temperature or spraying dispersity. In this study, the impact of the carrying gas flow temperature and the droplet slipping velocity $w_{l,g}$ was evaluated. The focus was given to water spraying under a wide range of flue gas temperatures $T_g \equiv 633 \rightarrow 1833$ K in power plants, where a cleaned vapour condensate of 313 K temperature from an economiser is often used.

An average humidity flue gas flow is a flow with a velocity of 10 m/s and a water vapour volume fraction of $X_v \equiv 0.25$, in which medium-sized droplets having $2R_0 = 500$ μm diameter evaporate within the gas flow. The droplet slipping velocity in an airflow is defined according to the initial Reynolds number $\mathrm{Re}_0 \equiv 1 \rightarrow 100$, which rapidly decreases in the transitional phase change regime (Fig. 7a). The role of the slipping factor in the phase transfer interaction is evaluated in terms of its influence on the thermal and energetic droplet states. The impact of slipping on the droplet's external and convective heating (Fig. 7b) directly affects the droplet, while the impact on the internal convective heating (Fig. 8a, b) affects it indirectly through forced water circulation due to friction forces. The intensity of water circulation inside the droplet is defined by the effective heat conductivity parameter (Fig. 8c), which changes due to Peclet number variations (Fig. 8d).

The convective heat flux $q_{c,l}$ defines the heat flux ratio $q_{c,l}/q_{c,g}$, which replaces the heat flux ratio $q_{r,l}/q_{c,g}$ in the heat transfer B_T parameter at expression (7) and makes it universal in the whole transitional phase change regime. Therefore, at the initial phase change stage, the heat flux

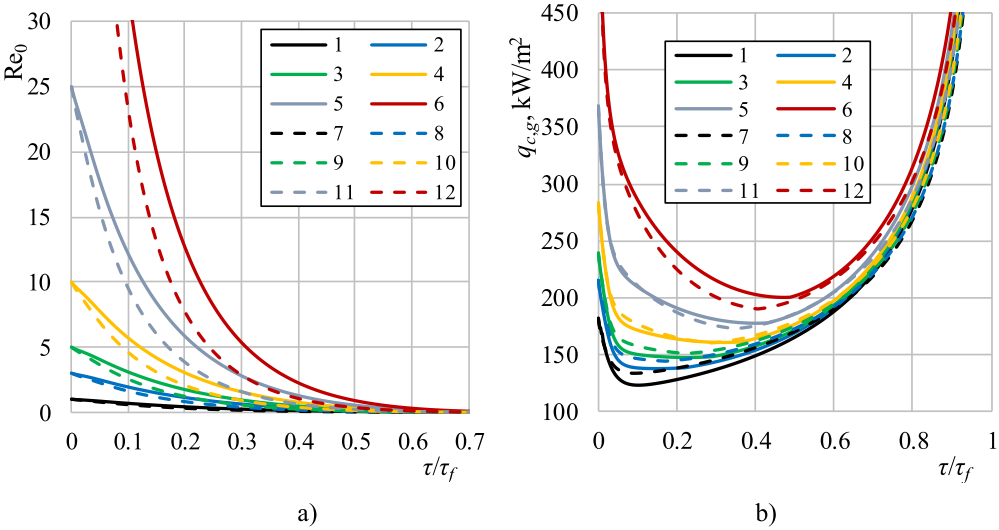

Fig. 7. Time history of Reynolds number (a) and convective flux $q_{c,g}$ (b) in the cases of combined "cr" (solid lines) and of convective "c" (dotted lines) heating. Re_0: (1,7) 1, (2,8) 3, (3,9) 5, (4,10) 10, (5,11) 25, (6,12) 100; $T_g = 1133$ K; $X_{v,g} = 0.25$; $2R_0 = 500$ μm; $T_{l,0} = 313$ K.

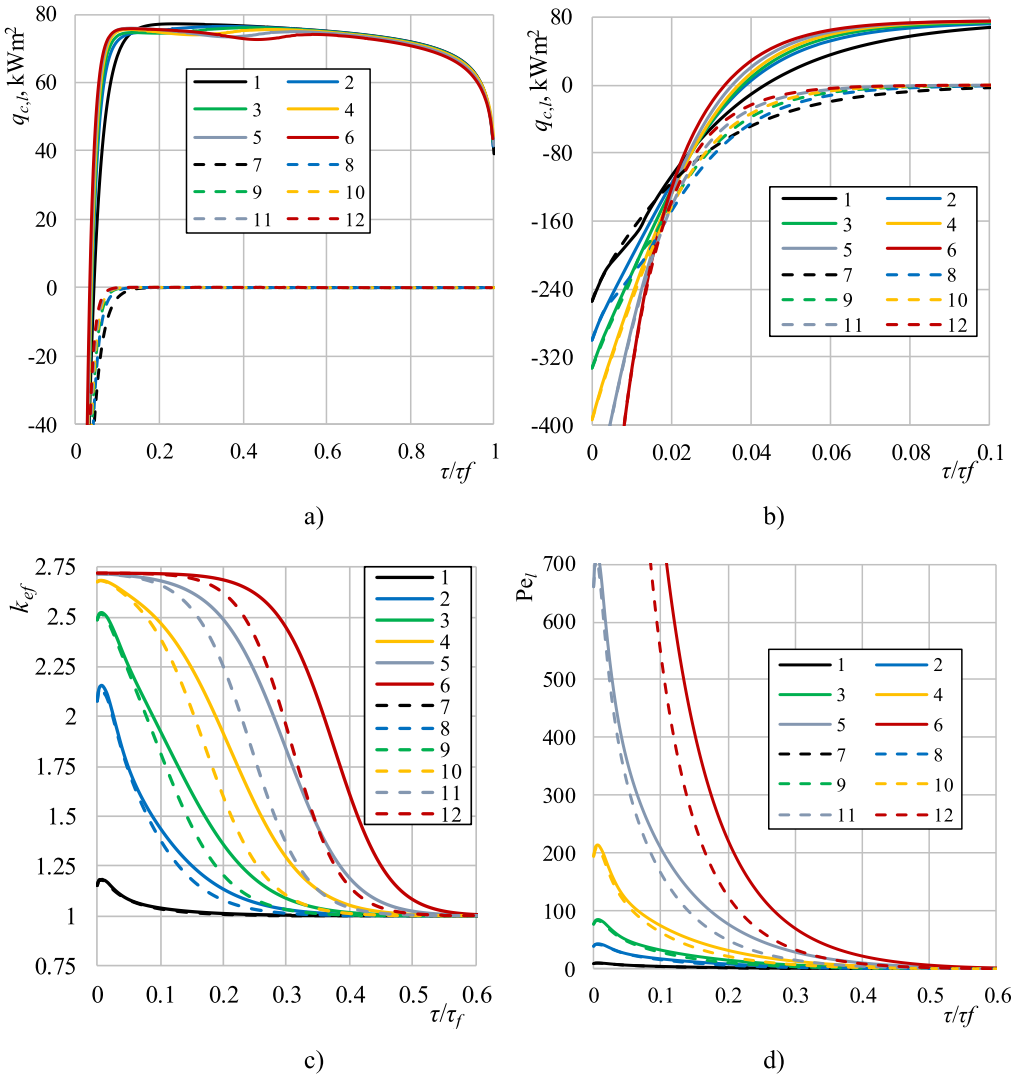

Fig. 8. Time history of convective flux $q_{c,l}$ in the cycle (4a) of phase change (a) and in its initial stage (b) and time history of parameter k_{ef} (c) and Peclet number (d). Markings as in Fig. 7.

dynamics $q_{c,l}$ (Fig. 8b) are significant in defining the transfer process interaction. In all modelled cases, the dew point temperature T_{dp} is 25.2 K higher than the water temperature $T_{l,0} = 313$ K. Thus, the droplet phase change cycle (4a) starts with the condensation regime, and the calculated vapour flux at the beginning is negative (Fig. 9a).

In the condensation regime, all the heat released in the condensation process is transferred inside the droplet by convection; therefore, the droplet warms rapidly to the dew point temperature (Fig. 9b). At the initial phase change stage, the droplet volume increases due to condensate and warming water expansion. At the onset of evaporation, the expansion of warming water still outweighs the impact of evaporation. Therefore, the droplet volume increases further until it reaches a maximum. When the effects of expansion and evaporation factors become equal, the volume has been increased by about 12–18% compared to the initial volume (Fig. 9c). Later in the evaporation regime, the droplet volume (Fig. 9c) and the surface area (Fig. 9d) decrease steadily, while at the end of the equilibrium evaporation, the droplet surface area changes linearly (Fig. 9d), independently from the heating process. This makes easier to define the dimensionless time scale τ/τ_f.

In the case of convective heating “c”, the impact of droplet slipping on its thermal state is negligible in the equilibrium evaporation (Fig. 9b dotted lines). In the case of combined “cr” heating, the slipping impact is more significant (Fig. 9b solid lines) and has the opposite effect (the position of curves in the “cr” case changes). The lowest calculated temperature is $T_{R,e,\text{“c”}}$, when $\text{Re}_0 = 1$. When the Reynolds number, which defines the slipping intensity, increases 100 times, the temperature $T_{R,e,\text{“c”}}$ increases only by 0.23 K. In the combined heating case “cr” when $\text{Re}_0 = 1$, the temperature $T_{R,e,\text{“cr”}}$ is the highest and equal to 358.5 K. When the Reynolds Re_0 number increases 100 times, the temperature $T_{R,e,\text{“cr”}}$ decreases by 1.34 K (Fig. 9b).

The droplet evaporation is the fastest when $\text{Re}_0 = 100$ (Fig. 9a): $g_{v,\,max,\,\text{“c”}} = 0.1$ mg/s and $g_{v,max,\,\text{“cr”}} = 0.125$ mg/s. In the combined heating case “cr”, the increase in the droplet evaporation intensity (Fig. 9a) and thermal state (Fig. 9b) is explained by the direct radiation impact. In the “c” heating case, the equilibrium evaporation thermal state insensitivity for droplet slipping confirms that convective heating intensity with increasing slipping velocity (Fig. 7b) is compensated by the increased evaporation rate (Fig. 9a). This means that in water droplets’ phase change cycle regimes (4a), there is a complex interaction between heat and mass transfer processes. For its intensity, the important factor is the competing impact of radiation absorption in semi-transparent droplets and their slipping in the flue gas flow and evaporation (Fig. 10). Since the flue gas flow temperature significantly impacts the droplet’s slipping dynamics (Fig. 10b) and radiation absorption (Fig. 10a) and evaporation (Fig. 10c, d) the gas temperature becomes an essential factor in the

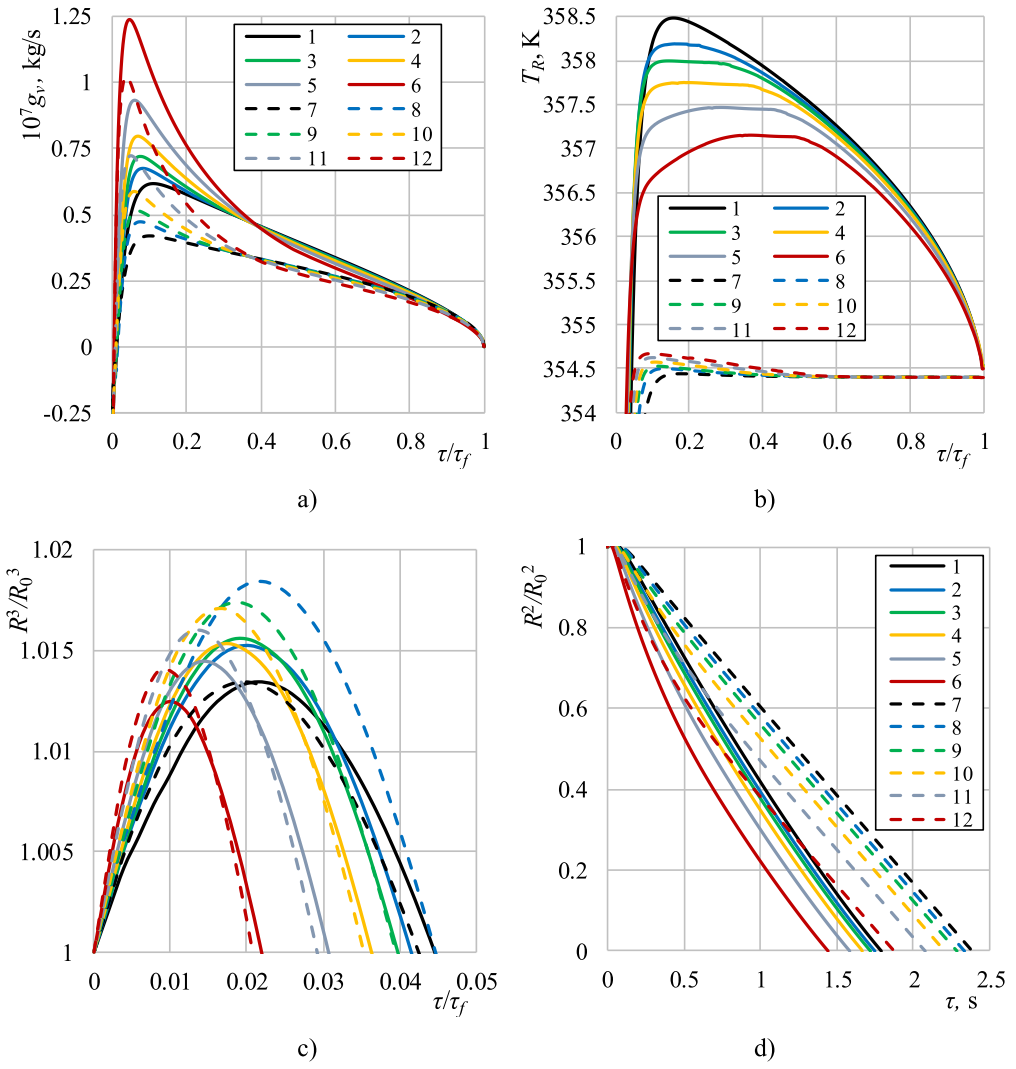

Fig. 9. Time history of vapour flux (a) and droplet surface temperature (b), of droplet evaporation dynamics R^3/R_0^3 (c) and R^2/R_0^2 (d). Markings as in Fig. 7.

interaction between multiple transfer processes.

The competing effects of droplet slipping and radiation absorption inside a droplet can be seen in the dynamics of both average mass temperature and enthalpy, as their trends are qualitatively the same (Fig. 11a, b). In the modelled cases $T_e > T_{l,0}$, the droplet initially heats up intensively and reaches the first maximum of the temperature (Fig. 11a) and enthalpy (Fig. 11b). The latter is influenced by the air flow temperature T_g and the heating process. In the convective heating case "c", independent from the airflow temperature T_g, the droplet temperature and enthalpy decrease slightly but steadily (Fig. 11a, b dotted lines) because the droplet slipping velocity decreases rapidly due to the impact of drag forces. In the combined "cr" heating case, it can be observed only in the low-temperature T_g 633 K case (Fig. 11a, b line 1). For the higher T_g case, the radiation impact increases, and the graphs of functions $T_{l,m}(\tau)$ and $h_l(\tau)$ become more complex. They clearly show the formation of a second maximum in temperature and enthalpy during the droplet's evaporation (Fig. 11a, b lines 3–5).

At the temperature of 933 K, the T_g case is considered intermediate, as the tendency for second peak formation is evident (Fig. 11, b, line 2). However, in a strict assessment, one maximum remains. The formation of the maximum in functions $T_{l,m}(\tau)$ and $h_l(\tau)$ graphs is related to the opposite effect of water circulation inside the droplet and the radiation absorption factor: the absorption of the radiation increases the non-isothermal state inside the droplet, while water circulation suppresses it. The first maximum forms in the transitional evaporation regime when droplet slipping factors overcome the radiation factor. This is influenced by the formation of a negative temperature field gradient inside the droplet (Fig. 11c).

When a negative temperature gradient forms inside the droplet, the radiation starts to participate in the surface water evaporation. This favours a temporary decrease in the droplet's mass average temperature and enthalpy. It is important to highlight that when the droplet's velocity steadily approaches the flue gas flow velocity, the water circulation inside the droplet ends (Fig. 10b). As a result, the temperature of the droplet starts to rise again because of the impact of the radiation flux participating in heating the water. The decrease in the evaporating droplet means that radiation absorption in it also decreases (Fig. 10a). This allows for the droplet to cool down and causes the formation of a second maximum in the graphs of functions $T_{l,m}$ (τ) (Fig. 11a) and $h_l(\tau)$ (Fig. 11b). Hence, radiation absorption in semi-transparent liquid causes a distinctive change in its thermal and energy state and thus directly influences the phase change rate.

For the interaction between combined heat transfer processes, radiation absorption inside the droplet depends on its size and the radiation source temperature (Fig. 12). As the phase transformation proceeds, the droplet becomes smaller and more transparent, while the local radiation flux becomes more evenly distributed inside the droplet as the temperature source increases (Fig. 12). This can be seen in the case of a high-

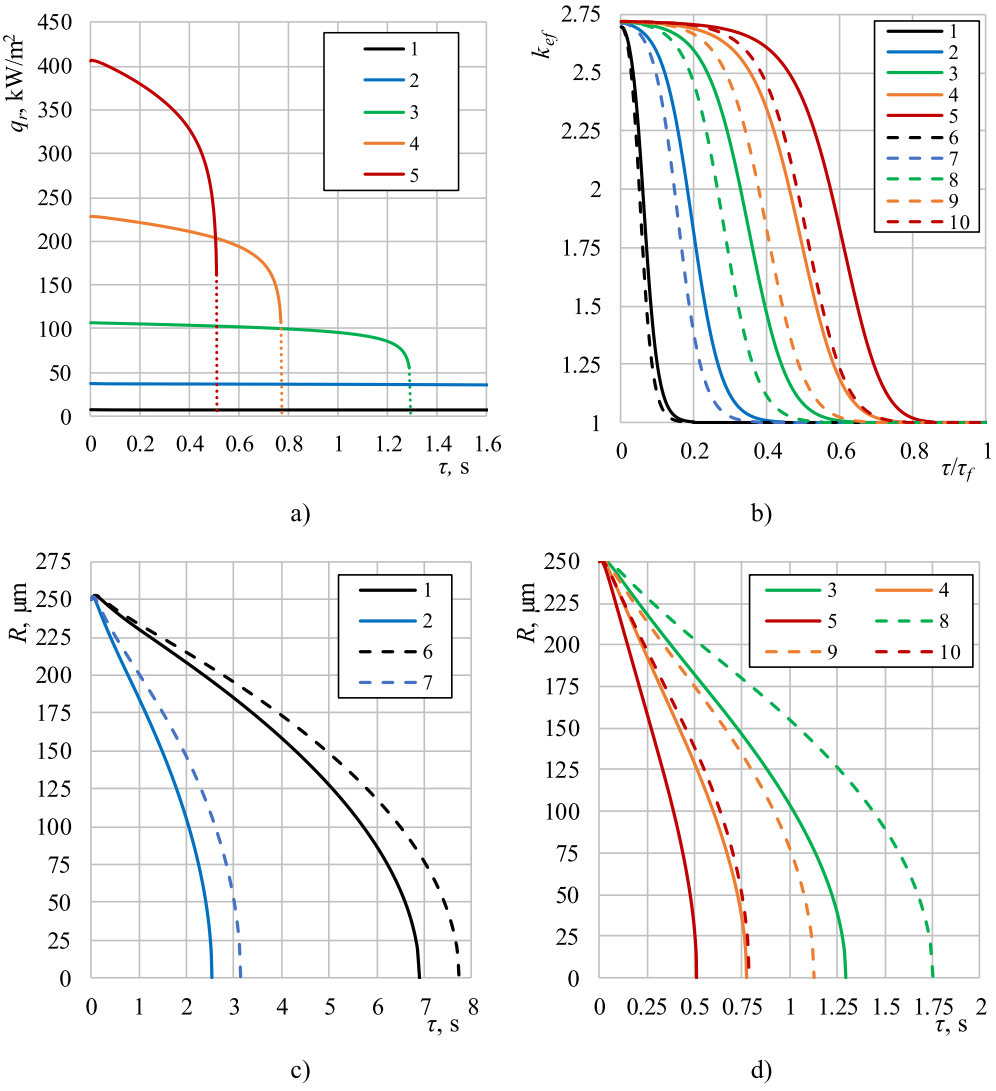

Fig. 10. Time history of absorbed radiation flux (a), effective conductivity parameter (b) in the water droplet and its evaporation (c, d) for different temperature air flow in the cases of combined heating "cr" (solid lines) and of convective heating "c" (dotted lines). T_g, K: (1,6) 633, (2,7) 933, (3,8) 1233, (4,9) 1533, (5,10) 1833; $\mathrm{Re}_0 = 25$; $X_{v,g} = 0.25$; $2R_0 = 500$ μm; $T_{l,0} = 313$ K.

temperature source, when the radiation absorption is significantly more uniform in large droplets (Fig. 12d). Some turns could be observed in the curves of local dimensionless flux functions $q_r(\eta)/q_r(\eta = 1)$ (Fig. 12). Apparently, they form due to the impact of light beam reflection at the internal droplet surface, which is significantly influenced by Brewster's angle variation (Fig. 13a) and the changing peculiarities of water's light spectral absorption coefficient (Fig. 13b). The flattening of local dimensionless radiation flux curves $q_r(\eta)/q_r(\eta = 1)$ with the increasing source temperature (Fig. 12 a-d) could be caused by the changes in water spectral properties (refractive index (Fig. 14a) and the absorption index (Fig. 1b lines 4–6)), when the maximum of the Planck function shifts to the shorter wavelength region (Fig. 14b lines 7–11) with increasing source temperature.

The absorption peculiarities inside droplets impact the convective heating ratio $q_{c,l}/q_{c,g}$ (Fig. 15a, b), which defines the Spalding heat transfer parameter B_T (Fig. 15c), which evaluates the influence of Stefan's hydrodynamic flow on external convective heating. The radiation impact on the Spalding mass transfer parameter B_M (Fig. 15b), and which evaluates the effect of Stefan hydrodynamic flow in convective evaporation, is indirect and is revealed through changes in the droplet surface temperature T_R (Fig. 9b).

The impact of Spalding B_T and B_M parameter versatility on Stefan hydrodynamic flow in phase change regimes is ensured by convective heat flux vector changes and energy origin transformations in droplets phase change cycle (4a). The direction of the heat flux $q_{c,l}$ vector inside the droplet is unambiguously defined by the temperature gradient: as long as the temperature gradient is positive, heat spreads into the droplet by internal convection.

In the condensation regime, the temperature gradient is positive regardless of the droplet heating case; therefore, $q_{c,l}$ by its nature corresponds to the sum of condensation heat flux $q_{f\equiv co}$ and convection heat flux $q_{c,g}$. At the time τ_{co}, the heat flux $q_{c,l}$ is equal to the convective heat flux $q_{c,g}$ provided to the droplet.

The end of the condensation regime τ_{co} is defined as the moment when the vapour flux reaches zero value, indicating a transition in the phase regime (Fig. 9a). In the case of convective heating "c", at the end of the transitional evaporation regime $\tau \equiv \tau_{co} \rightarrow \tau_e$, the heat flux $q_{c,l}$ corresponds to the part of heat flux $q_{c,g}$ that warms the droplet. It becomes zero at the time τ_e (Fig. 15b dotted lines). In the combined heating case "cr" in the transitional evaporation regime, two characteristic periods of transitional evaporation can be distinguished. They are separated at the time τ_r where the temperature gradient equals zero (Fig. 11d solid lines). At the first period $\tau \equiv \tau_{co} \rightarrow \tau_r$, the heat flux $q_{c,l}$ flows inside the droplet

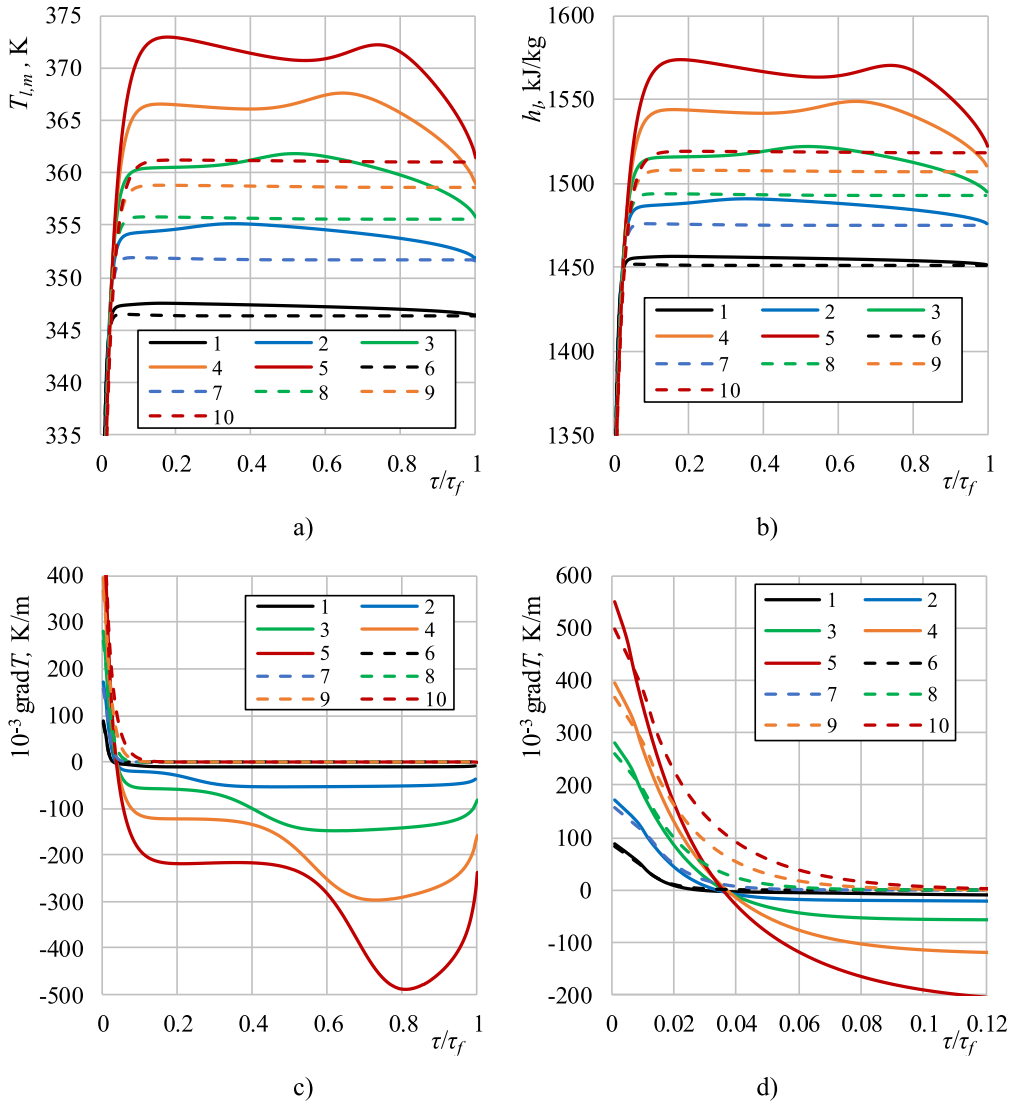

Fig. 11. Time history of droplet mass average temperature (a), enthalpy (b) and of droplet temperature gradient (c, d). Markings as in Fig. 10.

and by its nature corresponds to the part of convection $q_{c,g}$ that warms water. The latter is equal to zero at the time τ_r. During the second period, the $\tau \equiv \tau_r \rightarrow \tau_e$ temperature gradient is negative; therefore, heat flows to the droplet surface by internal convection, and the heat flux $q_{c,l}$ is equal to the part of radiation flux that is involved in surface water evaporation. At the time τ_e, the second maximum forms in the graphs of the functions $T_{l,m}(\tau)$ (Fig. 11b) and $h_l(\tau)$ (Fig. 11b), and then $q_{c,l}$ equals the radiation flux $q_{r,l}$ absorbed by the droplet. In the equilibrium evaporation regime $\tau \equiv \tau_e \rightarrow \tau_f$, the convection heat flux $q_{c,l}$ is enhanced by a heat flux $q_{l,h}$ proportional to the enthalpy change in the cooling droplet, therefore:

$$q_{c,l}\left(\tau \equiv \tau_e \rightarrow \tau_f\right) = q_{r,l}(\tau) + q_{l,h}(\tau), q_{l,h} = -\frac{1}{3}\rho_l c_{p,l} R \frac{dT_{l,m}}{d\tau} \quad (29)$$

In the modelled cases of a relatively cold water spray $T_e/T_{l,0} > 1$, the contribution is negligible for convective heating "c", while for the combined heating case "cr", the change in the enthalpy is more significant (Fig. 11b solid lines). Therefore, the evaporation is accelerated. In the case of hot water spraying $T_e/T_{l,0} < 1$, the enthalpy change contribution for intensively cooling droplets will be significantly higher. The interaction between combined transfer processes for the case $T_e/T_{l,0} < 1$ could only be defined by an additional investigation.

4. Conclusions

After establishing the applicability limit of the spectral radiation model based on the theory of geometric optics for semi-transparent droplets with diameters 2 R > 20 μm, and improving the numerical research methodology for droplet evaporation modelling by fully accounting for the influence of the heating droplet temperature on the physical-spectral optical properties of water, the results of the numerical simulation of phase changes in water droplets in flue gas flow at 673–1873 K can be summarised as follows:

1. In a flue gas flow, the phase changes of sprayed water droplets are defined by the variations in their surface temperature, which not only depend on the flue gas flow parameters but are also influenced by the water temperature and the droplet heating process, where droplets slipping and spectral radiation absorption play an exceptional role.
2. The thermal and energetic dynamics of the droplets cannot be predicted unambiguously from the sensory temperature, because the

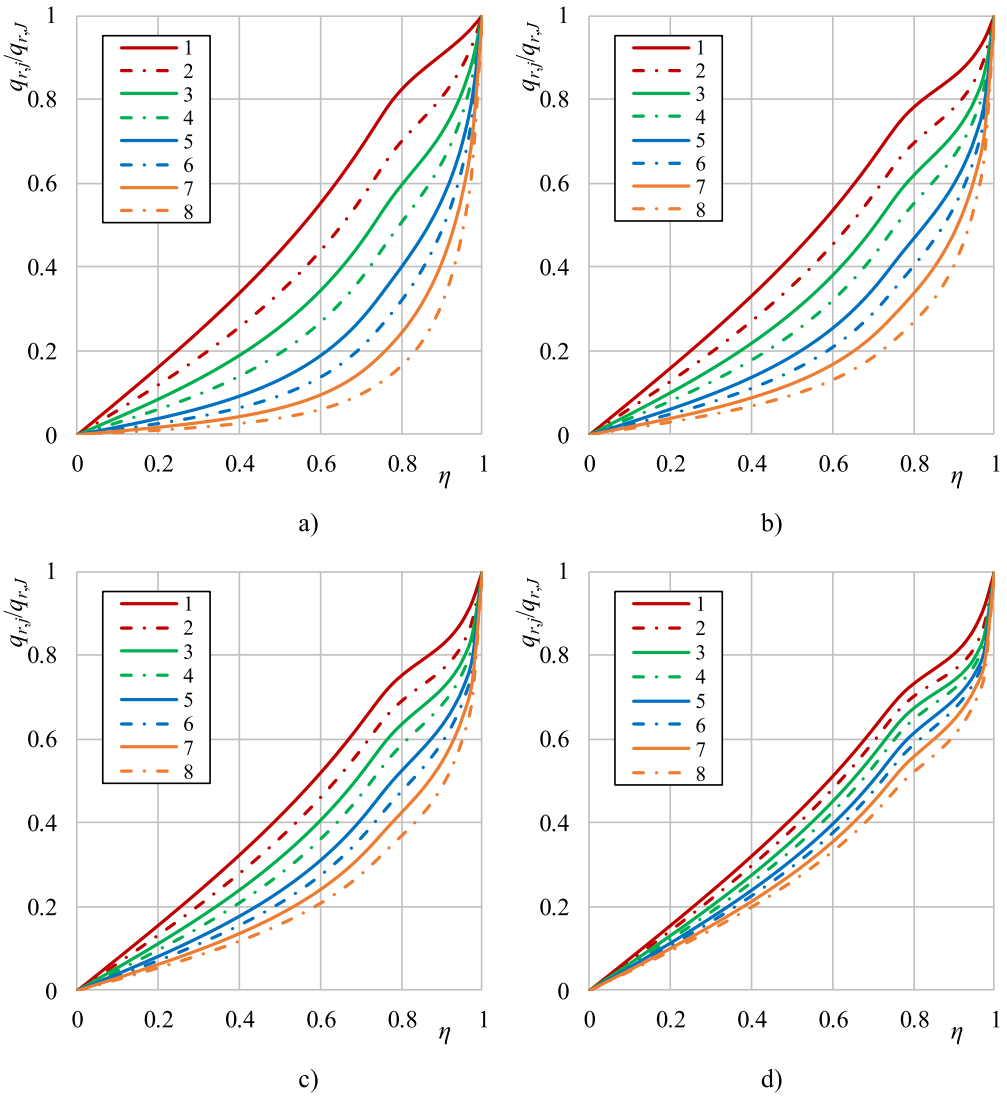

Fig. 12. The local radiative heat flux dependence on water droplet size and radiating source temperature T_{sour}, K: 663 (a), 933 (b), 1233 (c) and 1833 (d).R/R_0: (1) 0.1, (2) 0.2, (3) 0.3, (4) 0.4, (5) 0.55, (6) 0.7, (7) 0.9, (8) 1; $2R_0 = 500$ μm; $T_{l,0} = 313$ K; $\mathrm{Re}_0 = 25$; $X_{v,g} = 0.25$; $T_g = T_{sour}$.

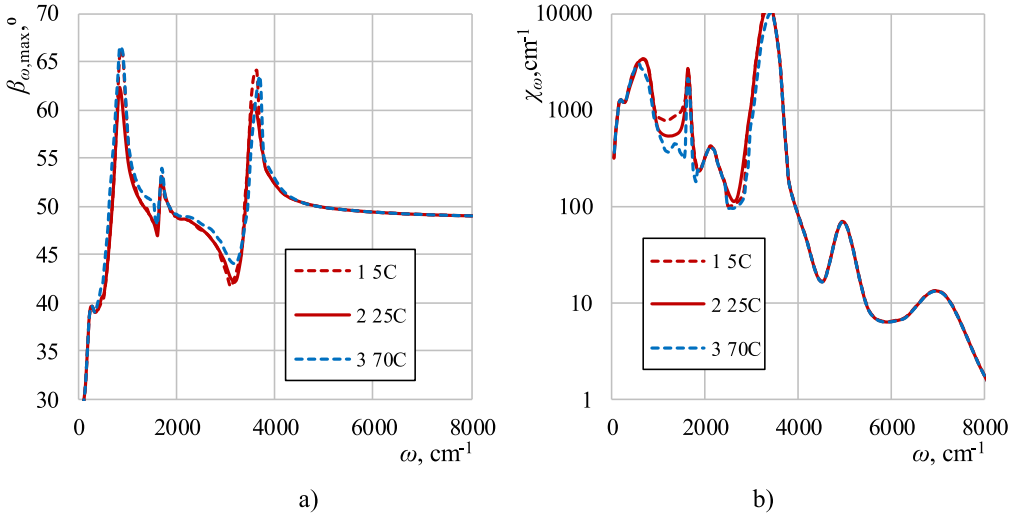

Fig. 13. Brewster spectral angle (a) and spectral absorption coefficient (b) for water. T_l, K: (1,3) 278, (2) 298; $\bar{n}_\omega = n_\omega - ik_\omega$: (1,3) data [32], (2) data [33].

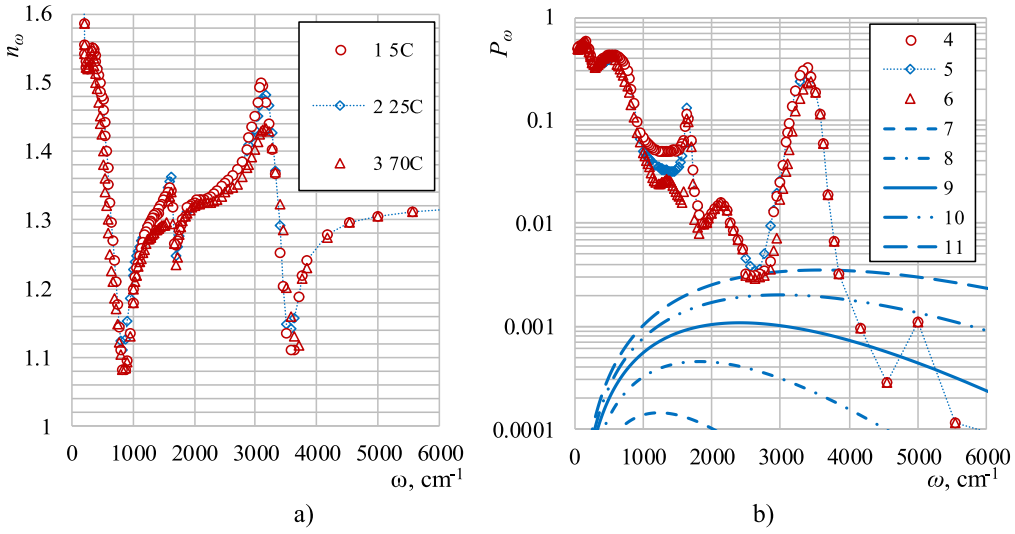

Fig. 14. Spectral index of refraction (a), spectral absorption index (b line 4–6) of water and Planck function (b lines 7–11), when T_{sour}, K: (7) 633, (8) 933, (9) 1233, (10) 1533, (11) 1833; T_l, K: (1,3,4,6) 278, (2,5) 298; Parameter P_ω: (4–6) k_ω, (7–11) $I_{\omega 0}$; $\bar{n}_\omega = n_\omega - ik_\omega$: (1,3,4,6) data [32], (2,5) data [33].

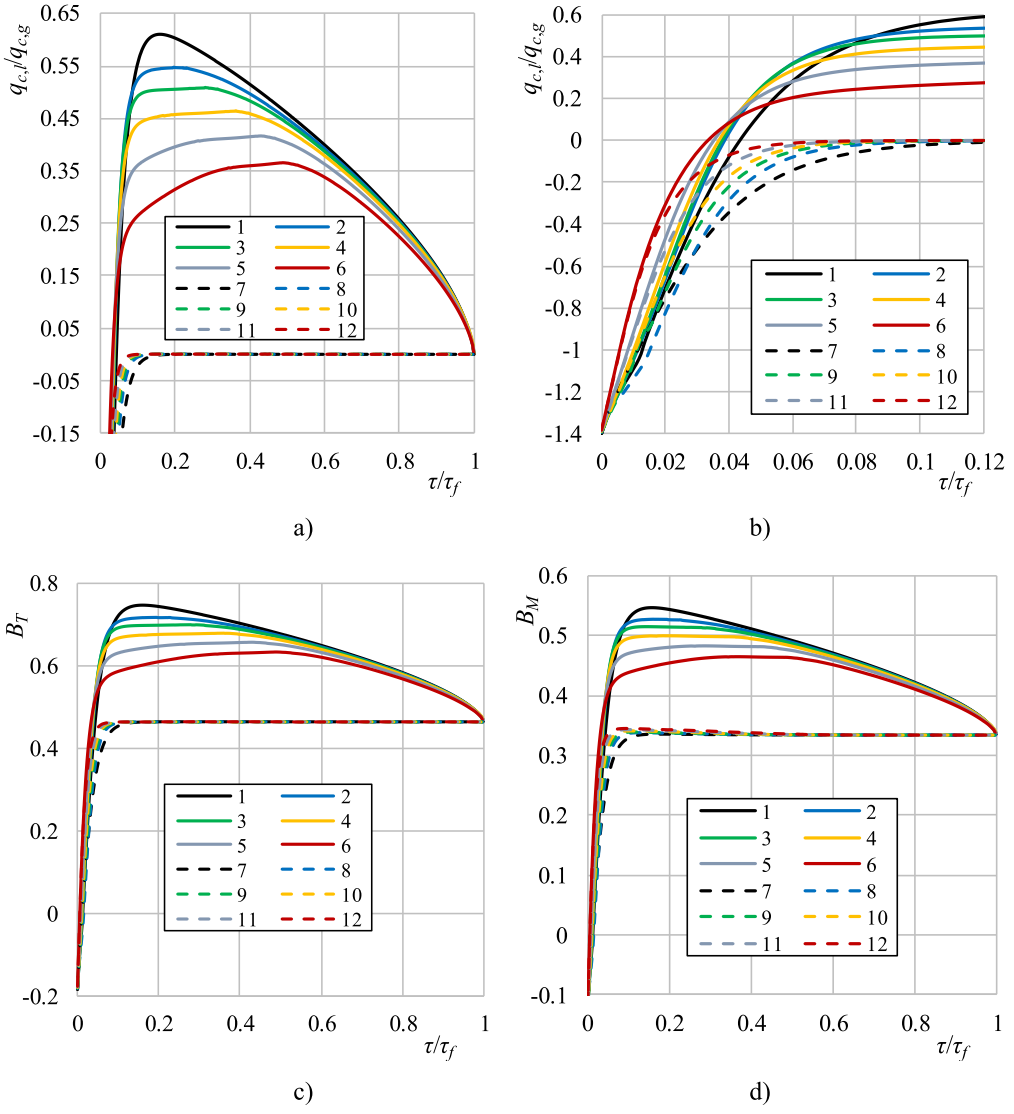

Fig. 15. Time history of heat flux's ratio $q_{c,l}/q_{c,g}$ (a, b) and Spalding heat parameters B_T (c) and B_M (d). Markings as in Fig. 7.

droplet heating process and the equilibrium evaporation temperature need to be taken into account as well.

3. For the droplets in equilibrium evaporation, the temperature *Te* is defined by the flue gas flow temperature and humidity as well by the droplet heating process. Therefore, the sprayed water temperature T_l has no direct impact on the temperature T_e. However, the temperature T_e determines phase change regimes, while the ratio T_e/T_l determines the droplet's heating/cooling in the transitional evaporation regime.
4. The role of radiation in the interaction between transfer processes in a semi-transparent water droplet is revealed through the droplet's non-isothermal state and internal temperature gradient changes, both of which depend significantly on the radiating source temperature and the droplet's size. Due to the effect of radiation, large water droplet evaporation intensifies by more than double in the 818 K temperature air and up to four times in the 1133 K temperature air.
5. The competing influence of droplet slipping and radiation absorption by the droplets is essential for the interaction between transfer processes. Droplet slipping affects convective heating, while internal convective heat transfer is indirectly affected by the forced circulation of the water caused by frictional forces. It is noted that droplet slipping is rapidly terminated due to drag forces. The absorbed radiation heat flux directly affects the heating of internal droplet layers and only enters the surface evaporation process when a negative temperature gradient forms. The influence of radiation is weakened in the final evaporation stage due to the rapid decrease in droplet size.
6. The peculiarities of spectral absorption inside water droplets define the ratio of convective heat fluxes $q_{c,l}/q_{c,g}$, which directly affects the contribution of the Stefan flow to external convective heating, as evaluated by the Spalding heat transfer parameter B_T. The radiation influence on the Spalding mass transfer parameter B_M, which evaluates the Stefan hydrodynamic flow for convective evaporation, is indirect and is revealed through changes in the dynamics of droplet surface temperatures T_R.

Nomenclature

a – thermal diffusivity, m^2/s;.
B_M — Spalding mass transfer parameter;.
B_T — Spalding heat transfer parameter;.
c_p – mass specific heat, J/(kg K);.
D – mass diffusivity, m^2/s;.
Fo – Fourier number;.
g_v — vapour mass flux, kg/s;.
h – enthalpy, J/kg;.
H – enthalpy, J;.
I_ω — intensity of spectral radiation, W/(cm ster)];.
$I_{\omega 0}$ — intensity of black body spectral radiation, W/(cm ster)];.
k_{ef} – effective conductivity parameter;.
k_ω – spectral index of absorption;.
L – latent heat of evaporation, J/kg;.
m – vapour mass flux density, kg/(m^2s);.
n – number of the term in infinity sum;.
n_ω – spectral index of refraction;.
$\overline{n}_\varpi$ – complex refractive index;.
Nu– Nusselt number;.
p – pressure, Pa;.
P – symbol of free parameter in droplet heat-mass transfer;.
Pe — Peclet number;.
q – heat flux, W/m^2;.
r– radial coordinate, m;.
Pr — Prandtl number;.
R — radius of a droplet, m;.
Re – Reynolds number;.
Sc — Schmidt number;.
Sh — Sherwood number;.
T – temperature, K;.
w_g – gas flow velocity, m/s;.
w_l – droplet velocity, m/s;.
$w_{l,g}$ – droplet slipping velocity in to gas flow, m/s;.
$w_{l,R}$ – water maximum velocity on the droplet surface, m/s.
X_v — vapour molar/volumetric fraction;.
Y_v — vapour mass fraction.

Greek symbols:

α_{ef} – absorptance;.
$\beta_{\omega,\max}$ – Brewster angle, rad;.
β and γ – angles, estimating the peculiarities of spherical geometry when calculating radiation in droplet, rad;.
δ – relative error, $^\circ/_o$;.
ε – emissivity;.
η – non-dimensional radial coordinate;.
θ – angle between the opposite direction of the normal to the surface element and incident beam, rad;.
$\kappa_{\omega,\beta}$ – spectral reflection coefficient;.
λ – thermal conductivity, W/(m K);.
ρ – density, kg/m^3;.
σ – Stefan-Boltzmann constant, W/(m^2K);.
τ – time, s;.
ψ – angle of light beam descent, rad;.
ω – wave number, cm^{-1}.

Subscripts.

c – convective;.
co – condensation;.
dp — dew point;.
dry – dry;.
e — equilibrium evaporation;.
ef — effective;.
f – phase change;.
g – gas;.
i – time index in a digital scheme;.
I – index of control time;.
it – index of iteration;.
IT – index of final iteration;.
j – index of radial coordinate;.
J – index of droplet surface;.
l – liquid;.
m – mass average;.
r – radiative;.
R – droplet surface;.
s – saturation;.
sour – source of radiation;.
v – vapour;.
vg – gas-vapour mixture;.
0 – initial state.

Funding

This research did not receive any specific grant from funding agencies in the public, commercial, or not-for-profit sectors.

CRediT authorship contribution statement

Robertas Poškas: Writing – review & editing, Formal analysis. **Monika Maziukiene:** Writing – original draft, Methodology. **Gintautas Miliauskas:** Writing – original draft, Software, Investigation, Conceptualization. **Hussam Jouhara:** Writing – review & editing. **Egidijus Puida:** Writing – review & editing, Visualization, Formal analysis.

Declaration of Competing Interest

The authors declare that they have no known competing financial

interests or personal relationships that could have appeared to influence the work reported in this paper.

References

[1] C.C. Tseng, R. Viskanta, Enhancement of water droplet evaporation by radiation absorption, Fire Saf. J. 41 (2006) 236–247, https://doi.org/10.1016/j.firesaf.2006.01.001.

[2] Y. López, J. Obando, C.E. Uribe, A.A. Amell, Experimental and numerical study of the effect of water injection into the reaction zone of a flameless combustion furnace, Appl. Therm. Eng. 213 (2022) 118634, https://doi.org/10.1016/j.applthermaleng.2022.118634.

[3] W. Gao, M. Liu, J. Yin, Y. Zhao, W. Chen, J. Yan, An improved control strategy for a denitrification system using cooperative control of NH_3 injection and flue gas temperature for coal-fired power plants, Energy 282 (2023) 128759, https://doi.org/10.1016/j.energy.2023.128759.

[4] M. Stein, V. Bykov, U. Maas, Reduced simulation of the evaporation and decomposition of droplets and films of urea-water solution in exhaust gas environment, Proc. Combust. Inst. 38 (2021) 6687–6694, https://doi.org/10.1016/j.proci.2020.06.032.

[5] I. Voytkov, R. Volkov, P. Strizhak, Reducing the flue gases temperature by individual droplets, aerosol, and large water batches, Exp. Therm. Fluid Sci. 88 (2017) 301–316, https://doi.org/10.1016/j.expthermflusci.2017.06.009.

[6] G. Miliauskas, M. Maziukienė, H. Jouhara, R. Poškas, Investigation of mass and heat transfer transitional processes of water droplets in wet gas flow in the framework of energy recovery technologies for biofuel combustion and flue gas removal, Energy 173 (2019) 740–754, https://doi.org/10.1016/j.energy.2019.02.101.

[7] Chang-Eon Lee, Bong-Jin Yu, Do-Hyun Kim, Soo-Ho Jang, Analysis of the thermodynamic performance of a waste-heat-recovery boiler with additional water spray onto combustion air stream, Appl. Therm. Eng. 135 (2018) 197–205, https://doi.org/10.1016/j.applthermaleng.2017.11.060.

[8] N.A. Fuchs, Evaporation and Droplet Growth in Gaseous Media, Pergamon Press,, London, 1959.

[9] R. Clift, J.R. Grace, M.E. Weber, Bubbles, Drops and Particles, Acad. Press,, New York, 1978.

[10] H.C. Van de Hulst, Light Scattering by Small Particles, Dover Publ,, New York, 1981.

[11] C.F. Bohren, D.R. Huffman, Absorption and Scattering of Light by Small Particles, Wiley,, New York, 1998. DOI:10.1002/9783527618156.

[12] W.A. Sirignano, Fluid Dynamics and Transport of Droplets and Sprays, Cambridge University Press,, 2000, https://doi.org/10.1017/CBO9780511529566.

[13] L.A. Dombrovsky, D. Baillis, Thermal Radiation in Disperse Systems: An Engineering Approach, Begell House,, New York, 2010.

[14] S.S. Sazhin, Droplets and Sprays, Springer,, Heidelberg, 2014, https://doi.org/10.1007/978-1-4471-6386-2.

[15] G. Cossali, S. Tonini, Drop Heating and Evaporation: Analytical Solutions in Curvilinear Coordinate Systems, Springer,, 2021, https://doi.org/10.1007/978-3-030-49274-8.

[16] S. Sazhin, Droplets and Sprays: Simple Models of Complex Processes, Springer,, 2022, https://doi.org/10.1007/978-3-030-99746-5.

[17] D. Spalding, Convective Mass Transfer, Edward Arnold Ltd,, London, 1963.

[18] J.R. Howell, M.P. Meng, K. Daun, R. Siegel. Thermal Radiation Heat Transfer, Seventh edition.,, CRC Press,, New York, 2021, https://doi.org/10.1201/9780429327308.

[19] L.A. Dombrovsky, The use of transport approximation and diffusion-based models in radiative transfer calculations, Comp. Therm. Sci. Int. J. 4 (2012) 297–315, https://doi.org/10.1615/ ComputThermalScien.2012005050.

[20] G.M. Harpole, Radiative absorption by evaporating droplets, Int. J. Heat. Mass Transf. 23 (1980) 17–26, https://doi.org/10.1016/0017-9310(80)90134-9.

[21] P.L.C. Large, R.H. Rangel, On the role internal radiation absorption in single droplet vaporization, AAIA Pap. 30th Aerosp. Sci. Meet. 0106 (1992) 1–19.

[22] H. Watanabe, R. Kurose, S. Komori, H. Pitsch, Effects of radiation on spray flame characteristics and soot formation, Combust. Flame 152 (2008) 2–13, https://doi.org/10.1016/j.combustflame.2007.07.021.

[23] L.A. Dombrovsky, V.P. Solovjov, B.W. Webb, Attenuation of solar radiation by a water mist from the ultraviolet to the infrared range, J. Quant. Spectrosc. Radiat. Transf. 112 (2011) 1182–1190, https://doi.org/10.1016/j.jqsrt.2010.08.018.

[24] M.Q. Brewster, Evaporation and condensation of water mist/cloud droplets with thermal radiation, Int. J. Heat. Mass Transf. 88 (2015) 695–712, https://doi.org/10.1016/j.ijheatmasstransfer.2015.03.055.

[25] B. Wu, X. Zhao, Radiation characteristics of water droplets in a fire-inspired environment: A Monte Carlo ray tracing study, J. Quant. Spectrosc. Radiat. Transf. 212 (2018) 97–111, https://doi.org/10.1016/j.jqsrt.2018.03.023.

[26] L.A. Dombrovsky, V.Y. Levashov, A.P. Kryukov, S. Dembele, J.X. Wen, A comparative analysis of shielding of thermal radiation of fires using mist curtains containing droplets of pure water or sea water, Int. J. Therm. Sci. 152 (2020) 106299, https://doi.org/10.1016/j.ijthermalsci.2020.106299.

[27] O.O. Oluwole, A. Gupta, B. Wu, X. Zhao, K.V. Meredith, Y. Wang, Nongray models for radiative absorption and anisotropic scattering by water droplets in fire CFD simulations, Fire Saf. J. 120 (2021) 103034, https://doi.org/10.1016/j.firesaf.2020.103034.

[28] G. Miliauskas, Interaction of the transfer processes in semitransparent liquid droplets, Int. J. Heat. Mass Transf. 46 (2003) 4119–4138, https://doi.org/10.1016/S0017-9310(03)00231-X.

[29] G. Miliauskas, V. Sabanas, Interaction of transfer processes during unsteady evaporation of water droplets, Int. J. Heat. Mass Transf. 49 (2006) 1790–1803, https://doi.org/10.1016/j.ijheatmasstransfer.2005.11.015.

[30] B. Wang, Y. Xuan, X. Han, Analysis on roles of thermal radiation to evaporation and combustion of fuel droplets, Int. J. Therm. Sci. 191 (2023) 108306, https://doi.org/10.1016/j.ijthermalsci.2023.108306.

[31] R.M. Fedorenko, D.V. Antonov, P.A. Strizhak, S.S. Sazhin, Time evolution of composite fuel/water droplet radii before the start of puffing/micro-explosion, Int. J. Heat. Mass Transf. 191 (2022) 122838, https://doi.org/10.1016/j.ijheatmasstransfer.2022.122838.

[32] G.M. Hale, M.R. Querry, Optical constant of water in the 200-nm to 200-μm wavelength region, Appl. Opt. 12 (1973) 555–563.

[33] G.M. Hale, M.R. Querry, A.N. Rusk, D. Williams, Influence of temperature on the spectrum of water, J. Opt. Soc. Am. 62 (1972) 1103–1108.

[34] M. Renksizbulut, R. Nafziger, X. Li, A mass transfer correlation for droplet evaporation in high-temperature flows, Chem. Eng. Sci. 46 (1991) 2351–2358, https://doi.org/10.1016/0009-2509(91)85133-I.

[35] G. Miliauskas, Regularities of unsteady radiative-conductive heat transfer in evaporating semitransparent liquid droplet, Int. J. Heat. Mass Transf. 44 (2001) 785–798, https://doi.org/10.1016/S0017-9310(00)00127-7.

[36] B. Abramzon, W.A. Sirignano, Droplet vaporization model for spray combustion calculations, Int. J. Heat. Mass Transf. 32 (1989) 1605–1618, https://doi.org/10.1016/0017-9310(89)90043-4.

[37] G. Miliauskas, M. Maziukienė, R. Poškas, H. Jouhara, Peculiarities of thermal and energy state variation in phase change regimes of water droplets in radiating biofuel flue gas flow, Energy 307 (2024) 132650, https://doi.org/10.1016/j.energy.2024.132620.

[38] A.A. Fedorets, E.E. Kolmakov, L.A. Dombrovsky, Experimental study of the effect of water salinity on the parameters of an equilibrium droplet cluster levitating over a water layer, Front. Heat. Mass Transf. 22 (2024) 1–14, https://doi.org/10.32604/fhmt.2024.049335.

[39] X. Xi, C. Cai, H. Liu, R. Wen, X. Ma, X. Song, Analytical and experimental study on binary droplet evaporation: inhibitory effect of adding mineral oil adjuvant to water, Int. Commun. Heat. Mass Transf. 142 (2023) 106630, https://doi.org/10.1016/j.icheatmasstransfer.2023.106630.

[40] L. Zhou, X. Shi, H. Jiang, Z. Xu, S. Li, W. Xu, An experimental study on the thermal radiation attenuation effect of water mist from flat fan nozzle, Therm. Sci. Eng. Prog. 39 (2023) 101634, https://doi.org/10.1016/j.tsep.2022.101634.

[41] G. Miliauskas, E. Puida, R. Poškas, V. Ragaišis, L. Paukštaitis, H. Jouhara, L. Mingilaitė, Experimental investigations of water droplet transient phase changes in flue gas flow in the range of temperatures characteristic of condensing economizer technologies, Energy 256 (2022) 124643, https://doi.org/10.1016/j.energy.2022.124643.

[42] G.V. Kuznetsov, M.V. Piskunov, N.E. Shlegel, P.A. Strizhak, Experimental research of the vapor zone between two coalescing droplets of heated water, Int. Commun. Heat. Mass Transf. 126 (2021) 105410, https://doi.org/10.1016/j.icheatmasstransfer.2021.105410.

[43] L.A. Dombrovsky, A.A. Fedorets, V.Y. Levashov, A.P. Kryukov, E. Bormashenko, M. Nosonovsky, Stable cluster of identical water droplets formed under the infrared irradiation: experimental study and theoretical modeling, Int. J. Heat. Mass Transf. 161 (2020) 120255, https://doi.org/10.1016/j.ijheatmasstransfer.2020.120255.

[44] X. Luo, L. He, H. Wang, H. Yan, Y. Qin, An experimental study on the motion of water droplets in oil under ultrasonic irradiation, Ultrason. Sonochem. 28 (2016) 110–117, https://doi.org/10.1016/j.ultsonch.2015.07.004.

[45] M. Ivanov, E.V. Smirnova. Experimental research of liquid droplets evaporation velocity in non-moving high temperature environment. Trans. IGI, 1.

[46] G. Miliauskas, R. Poškas, E. Puida, H. Jouhara, Influence of sprayed water temperature on phase changes in droplets slipping in radiative flue gas flow of industrial biofuel boilers, Therm. Sci. Eng. Prog. 62 (2025) 103589, https://doi.org/10.1016/j.tsep.2025.103589.

[47] G. Miliauskas, A. Adomavicius, M. Maziukienė, Modelling of water droplets heat and mass transfer in the course of phase transitions. II: Peculiarities of the droplet radial coordinate and the time grid calibration, Nonlinear Anal. Model. Control 2 (2017) 135–151, https://doi./10.15388/NA.2017.3.7.